This manuscript is a pre-print of an article published in Basin Research with the published version available at https://onlinelibrary.wiley.com/doi/abs/10.1111/bre.12550

Principles of Shortening in Salt Basins Containing Isolated Minibasins

Oliver B. Duffy[1], Tim P. Dooley[1], Michael R. Hudec[1], Naiara Fernandez[1], Christopher A-L. Jackson[2], Juan I. Soto[1*]

[1]Bureau of Economic Geology, Jackson School of Geosciences, The University of Texas at Austin, University Station, Box X, Austin, Texas, 78713-8924, USA

[2]Basins Research Group (BRG), Department of Earth Science & Engineering, Imperial College, Prince Consort Road, London, United Kingdom, SW7 2BP

[*]On leave of absence from: Departamento de Geodinámica, Universidad de Granada, Avenida de Fuente Nueva s/n, 18071 Granada, Spain

Corresponding author: Oliver Duffy (oliver.duffy@beg.utexas.edu)

Abstract

Shortening styles in salt-influenced basins can vary markedly, with the volume and distribution of salt prior to shortening being a key control. Here we use a suite of physical models to examine styles of thin-skinned regional shortening in settings where the pre-shortening structure comprised minibasins surrounded by salt ('isolated-minibasin' provinces). Our models show that the high volume of mechanically-weak salt localizes lateral regional shortening, with shortening inducing salt flow towards the foreland that subsequently contributes to three key processes - translation, tilting and rotation of minibasins. First, we demonstrate that the flowing salt pushes against minibasins, propelling them in the regional shortening direction. Minibasin translation is enhanced by fast-flowing salt streams and impeded by basal friction due to welding and base-salt buttresses. Second, we show how minibasin tilt directions and magnitudes vary spatially and temporally during regional shortening. Minibasins tilt away from zones of pressurized salt, the

locations of which may shift due to changes in salt flow regimes. Tilt directions may also change as minibasins pivot on primary welds, or due to forces associated with minibasin collision. Third, minibasins can rotate around sub-vertical axes during regional shortening. We speculate that this rotation is caused by a combination of: i) traction imparted on the minibasin boundary by differential horizontal flow of adjacent salt; and ii) pivoting on primary and secondary welds. We synthesize our results in a series of 3-D conceptual models, before we compare and contrast regional shortening styles and processes in salt-influenced basins with different pre-shortening salt configurations. Our findings contribute to the understanding of the geometry and kinematics of shortened salt basins, as well as a deeper understanding of the tectono-stratigraphic evolution of minibasins.

1 Shortened Salt-Influenced Basins: Thin-Skinned Styles

Shortened salt-influenced basins are common in orogenic settings and in the down-dip contractional domains of salt-detached slope systems, displaying a wide range of structural styles (e.g. Davis and Engelder, 1985; Letouzey et al., 1995; Rowan and Vendeville, 2006; Callot et al., 2007; Morley et al., 2011; Lacombe and Bellahasen, 2016; Duffy et al., 2018; Granado et al., 2018; Legeay et al., 2019; Dooley et al., 2020; Hassanpour et al., 2020). This diversity in structural style arises during regional shortening due to: i) the strength difference between the relatively weak salt and relatively strong sedimentary rocks; ii) variations in the number and thickness of salt detachment levels, iii) the heterogeneous distribution of salt prior to shortening; and iv) variations in salt composition, rheology, and mobility. In particular, previous studies have shown how the proportion and distribution of mechanically weak salt in a system will significantly impact the structural styles that develop as it shortens (Davis and Engelder, 1985; Letouzey et al., 1995; Cotton and Koyi, 2000; Rowan and Vendeville, 2006; Callot et al., 2007; Dooley et al., 2009; Darnault et al., 2016; Duffy et al., 2017; 2018; Jackson and Hudec, 2017; Butler, 2019; Legeay et al., 2019). Three end-member configurations of salt typically exist prior to shortening: i) an undeformed flat- or gently-dipping salt layer; ii) an array of isolated stocks or walls encased in a relatively rigid sediment body ('isolated diapirs'; Duffy et al., 2018; Figure 1a); and iii) the focus of this study, settings where minibasins are surrounded by salt ('isolated minibasins'; Fig. 1b). Shortened isolated-minibasin settings have previously been termed Wall-and-Basin settings (WAB), and can include systems with multiple generations of minibasins and salt canopies (e.g. Axel-Heiberg Island, Arctic Canada [Jackson and Harrison, 2006; Harrison and Jackson, 2014]; the central portion of the Sivas Basin, Turkey [Kergaravat et al., 2017]). In this study we focus on styles of thin-skinned ('supra-salt') regional shortening, though we recognize that many shortened salt-influenced basins may have additional thick-skinned components (e.g. Legeay et al., 2019).

Where bedded salt is initially undeformed, a basal detachment can form within it during regional shortening, with a fold-and-thrust belt developing within its overburden (e.g. Davis and Engelder, 1985; Letouzey et al., 1995; Costa and Vendeville, 2002; Morley et al., 2011). Such thin-skinned fold-and-thrust belts are typically characterized by: i) an extremely low cross-sectional taper (≤1°), with folds and thrusts developed across a wide belt; ii) abrupt changes in structural style at the edges of the salt basin, where deformation is concentrated; iii) regularly-spaced, salt-bearing thrusts that do not display a consistent dominant vergence, broad, box-like synclines, and narrow, symmetric, salt-cored anticlines; and iv) a remarkable continuity of structural style, which may extend 10s or 100s of kilometers along-strike (e.g. Davis and Engelder, 1985; Letouzey et al., 1995; Morley et al., 2011) (Fig. 2). Natural examples of such settings include the Valley and Ridge Province of the Appalachians, USA (e.g. Frey, 1973), the Alps and the Jura Mountains, Switzerland and France (e.g. Laubscher, 1961; Guellec et al., 1990; Leitner and Spötl, 2017; Sommaruga et al., 2017), the Salt Range, Pakistan (e.g. Grelaud et al., 2002), the Sub-Andean foreland in Peru and Bolivia (e.g. Rodriguez et al., 2001; Hermoza et al., 2005; Baby et al. 2018; Iribarne et al., 2018; McClay et al., 2018), and the Northwestern Zagros Mountains, Iran (e.g. Sherkati et al., 2006; Dooley et al., 2007; Najafi et al., 2014; see Davis and Engelder, 1985 for a more complete list).

Where diapirs have formed prior to regional shortening, they preferentially localize shortening strain such that they narrow and rise as they are squeezed (Fig. 2b). In contrast, at low regional shortening strains, the comparatively strong surrounding sedimentary rocks remain mostly undeformed (e.g. Nilsen et al., 1995; Rowan and Vendeville, 2006; Callot et al., 2007; Dooley et al., 2009; 2013; Duffy et al., 2018; Legeay et al., 2019). Duffy et al (2018) synthesize how isolated-diapir provinces shorten using observations from published natural examples such as the Fars Region of the Zagros Mountains, Iran (e.g. Callot et al., 2007; 2012) and the Astrid Fold Belt in the Lower Congo Basin, Gabon (e.g. Jackson et al., 2008), as well as data from physical models (e.g. Callot et al., 2007; Dooley et al., 2009, 2015). They show that in shortened isolated-diapir systems, faults and/or folds typically nucleate at diapirs before propagating out into flanking sedimentary rocks (see also Snidero et al., 2019). These faults and/or folds connect with those from adjacent diapirs, or directly to other diapirs, forming a network (e.g. Callot et al., 2012; Duffy et al., 2018). The style and orientation of the faults and/or folds in the network is largely determined by the pre-shortening configuration of diapirs within the array (e.g. Callot et al., 2007; Dooley et al., 2009; Duffy et al., 2018). Duffy et al. (2018) surmise that the relatively low volume of salt, and the isolated and poorly-connected nature of the salt bodies in isolated-diapir settings, results in a thin-skinned system that behaves in a mechanically relatively rigid manner during regional shortening. Critically, shortened isolated-diapir settings show greater spatial variability in structural style than shortened settings developed above an initially undeformed salt decollement (*cf*. Davis and Engelder, 1985 and Duffy et al., 2018).

The relative wealth of knowledge on shortening styles in isolated-diapir settings is not matched for isolated-minibasin settings, where knowledge of the processes, kinematics, and controls during shortening is not yet fully-developed. Prior to shortening, settings such as the southeast portion of the Precaspian Basin, Kazakhstan (e.g. Duffy et al., 2017; Fernandez et al., 2017; Jackson et al., 2020) and the central portion of the Sivas Basin (central domain), Turkey (Ringenbach et al., 2013; Callot et al., 2014; Kergaravat et al., 2016; 2017; Ribes et al., 2017; Legeay et al., 2019), are interpreted to have had a high salt volume (Fig. 1b) with a polygonal network of salt walls surrounding isolated minibasins in map-view. Isolated-minibasin systems are less mechanically-rigid during regional shortening than isolated-diapir settings, given the minibasins are essentially disconnected from one another and mobile (e.g. Rowan and Vendeville, 2006; Legeay et al., 2019). As such the minibasins have the potential to behave independently, with significant implications for resulting structural styles (e.g. Rowan and Vendeville, 2006; Legeay et al., 2019). However, fundamental questions remain about how and why the mobile and isolated minibasins translate, tilt (i.e. around a horizontal axis) and rotate (i.e. around a sub-vertical axis) during regional shortening. To address these questions, we first review the fundamental mechanical principles that control structural styles developed in shortened isolated-minibasin provinces. We couple this review with observations from a suite of new physical models designed to explore key processes that occur as isolated minibasin provinces shorten – minibasin translation, tilting, and rotation. We then synthesise our findings in a series of 3D conceptual models. Finally, we assess the wider implications of our work, by comparing and contrasting shortening styles and processes in salt-influenced basins with different pre-shortening salt volumes and configurations. Our findings contribute to the growing body of literature highlighting how the geometry and kinematics of shortened salt basins are strongly controlled by the initial volume and distribution of salt.

2 Governing Principles and Characteristics of Shortened Isolated-Minibasin Provinces

The general principles of isolated-minibasin shortening are outlined by Rowan and Vendeville (2006). Using physical models, they show that regional shortening is preferentially accommodated by the weak salt surrounding the minibasins. In particular, pre-existing salt walls oriented perpendicular to the regional shortening direction narrow or weld out during shortening, with salt commonly extruded to feed a canopy. In contrast, walls oriented parallel to the regional shortening direction remain open and form strike-slip shear zones, whereas those oriented oblique to the regional shortening direction typically host oblique-slip transpressional shear zones (Rowan and Vendeville, 2006) (Fig. 3). As the salt deforms during regional shortening, the strong minibasins are mobile and translate independently of one another. Thus, minibasins may converge, diverge, and collide with minimal internal deformation, as well as rotate around horizontal and vertical axes (Rowan and Vendeville, 2006).

With these concepts in mind, and by looking for first-order diagnostic features, it could be possible to decipher if a salt basin formed in response to the shortening of an isolated-minibasin province. In map-view, diagnostic features include the presence of closely-spaced or welded, ovate minibasins. These minibasins may be bounded either by a polygonal to irregular network of salt walls, or an equivalent pattern of welds. Salt walls trending in one orientation tend to be narrower or preferentially welded-out, whereas those trending orthogonal tend to be wider (Fig. 3). Furthermore, the map-view distribution of extensional, contractional, and strike-slip deformation at the minibasin boundaries should be complex due to jostling between the mobile minibasins as they were packed close together (Fig. 3) (Rowan and Vendeville, 2006; Granado et al. 2018; Legeay et al., 2019). In section-view, diagnostic features can include the presence of internally-undeformed minibasins, extreme minibasin tilts, and highly spatially-variable structural styles (Rowan and Vendeville, 2006; Kergaravat et al., 2016, 2017; Duffy et al., 2017; Ribes et al. 2017; Legeay et al., 2019). Critically, structural restorations, salt volume estimates, and the tectono-stratigraphic history of the setting must be compatible with the principle of isolated minibasins having been initiated prior to regional shortening (e.g. salt volumes must be relatively high).

Shortened isolated-minibasin provinces occur in the SE Precaspian Basin, Kazakhstan (e.g. Duffy et al., 2017; Fernandez et al., 2017; Jackson et al., 2020), the central portion of the Sivas Basin, Turkey (Ringenbach et al., 2013; Callot et al., 2014; Kergaravat et al., 2016; 2017; Legeay et al., 2019), Axel-Heiberg Island, Arctic Canada (e.g. Harrison and Jackson, 2014), the Northern Calcareous Alps, Austria (Granado et al., 2018), the Betics, southern Spain (Flinch and Soto, 2017), the Flinders Range, South Australia (Rowan and Vendeville, 2006), and portions of contractional domains on the salt-detached slope above the Sigsbee canopy in the Northern Gulf of Mexico (Duffy et al. 2020; Fernandez et al. 2020a) (e.g. Fig. 4). However, fundamental questions remain regarding the thin-skinned processes that occur as isolated-minibasin provinces shorten. These questions include: 1) Why do minibasins translate and what factors may enhance or inhibit translation? 2) What factors influence the variable tilts we see in natural shortened isolated-minibasin provinces? (*cf*. Fig. 4c and d); and 3) Do minibasins rotate around vertical (or steep) axes, and if so, what factors influence this? To address these questions, we will present key observations from a suite of new physical models, highlighting the importance of salt flow, minibasin interaction, and base-salt relief.

.

3 Physical-Modelling Approach

In this paper we use the results of four physical models, with three different experimental setups, involving a variety of arrays of isolated minibasins sinking into a “sea” of salt to investigate processes such as minibasin mobility, minibasin tilting and minibasin rotation during regional shortening (Figure 5; see details below). As with other physical modeling studies of salt tectonics, we simulated halite using ductile silicone polymer and its siliciclastic overburden using brittle, dry, sands and hollow microspheres. The silicone was a near-Newtonian viscous polydimethylsiloxane (PDMS). This polymer has a density of 970 kg m^{-3} at room temperature and a dynamic shear viscosity of 2.5×10^4 Pa s at a laboratory strain rate of 3×10^{-1} s^{-1} (Vendeville and Jackson, 1992; Weijermars et al., 1993). In some of our models the salt analog was dyed with minute quantities of powdered pigments in order to track salt flow paths during model evolution (see Dooley et al., 2009, for further details). Our granular minibasin infills comprised different colored mixtures of silica sand with a bulk density of ~1,700 kg m^{-3}, grain size of 300-600 µm, internal friction coefficient, µ, of 0.55–0.65 (McClay, 1990; Krantz, 1991; Schellart, 2000), and hollow ceramic microspheres (“glass beads”) having a bulk density of 650 kg m^{-3}, an average grain size of 90-150 µm, and a typical µ of 0.45 (e.g. Rossi and Storti, 2003; Dooley et al., 2009). The glass beads serve to lower bulk grain size, as well as allow us to modify the bulk density of the suprasalt section. In all of our models the minibasins were initially seeded using outward-widening circular templates. Minibasins possessed a dense narrow core of our granular mixture with a density 1.4-times that of our salt analog, fringed by a wider circular template with a density 1.2-times that of our salt analog, and finally passing out into an outer fringe with a density equal to that of our salt analog. These densities were achieved by varying the ratio of sand to microspheres in the granular mixtures. This mimics natural minibasins which show denser cores due to increased burial and compaction in their cores relative to their fringes. Initially our minibasins possessed positive topography as the granular mixture was deposited using circular templates a on top of our salt analog, but the mixture sank over several hours to produce negative topography with a bowl-shaped profile. Thereafter, the negative relief of our minibasins were filled with granular materials up to top salt, firstly as they subsided into the salt basin and then as the salt massifs rose around the transported minibasins during shortening. Minibasin infills thus recorded the subsidence history as well as the tilting history of each individual minibasin. This “fill-to-top” approach inhibits minibasin encasement by salt sheets or a canopy above the minibasin array.

Computer-controlled cameras photographed the obliquely-lit upper and basal surfaces of the models at set time intervals of 3-10 minutes depending on the length of time of the experiment. A digital image correlation (DIC) system, consisting of a high-resolution stereo charge-coupled device system and associated software, tracked the surface-strain history, subsidence, and uplift values, as well as displacement vectors of the top, and in the case of Model 3, basal surfaces of the model, i.e. processed imagery from beneath the deformation looking up through the transparent base of the rig onto the base of the model. The speckled nature of the sand and cenosphere mixtures used in our models are ideal for this type of monitoring system (see Reber et al., 2020 for further details).

Adding syn-kinematic layers means data are incremental for individual layers deposited during subsidence and regional shortening stages of our models. We use two main types of DIC maps in this paper: (1) height-change maps that record minibasin tilting and the rise of salt, and: (2) maps showing displacement in the regional shortening direction (eastwards) that highlight fast and slow moving parts of the system. In all cases, where we show height change or displacement maps these values are incremental and are calculated over the period of the most recent minibasin infill cycle. For more details on DIC monitoring techniques the reader is referred to Adam et al. (2005). After completion, the models were impregnated with a gelatin mixture and left to partially dry for 12 hours, then, once sufficiently consolidated, sliced into closely spaced slabs (c. 3.5 mm apart). Coregistered digital photographs of these closely spaced serial sections yielded a 3D voxel of the completed model. Dip sections are the sliced and photographed cross sections, whereas strike sections, arbitrary lines and depth slices are virtual sections constructed from the voxel model. As a result, the strike section, arbitrary line and depth slice images are interpolated and thus not as sharp as those derived directly from photographed dip sections.

Salt withdrawal minibasins are typically 1-10 km in width (e.g. Hudec et al., 2009), and thus a scaling ratio of 2 x 10^{-5} (2 cm = 1 km) was employed in our experiments, yielding natural diameters of 3.5-8 km for our model minibasins (Fig. 5). The size of our model salt basins, or portion of salt basins, thus scales from 25-46 km long and 30 km wide (Fig. 5). Regional lateral shortening was applied using a moving endwall connected to a stepper motor system. Regional shortening was applied at a constant rate of 1.25 mm h^{-1} yielding strains rates between 3.6 x 10^{-7} s^{-1} and 7 x 10^{-7} s^{-1}.

The three model setups used in this study, which are schematically illustrated in Figure 5, were designed to test controls on shortening styles and minibasin behaviour that have been proposed based on studies of natural examples (e.g. Rowan and Weimer, 1998; Rowan and Vendeville, 2006; Callot et al., 2016; Duffy et al., 2017; Kergaravat et al., 2017; Legeay et al., 2019). Models 1a and b consisted of identical arrays of minibasins subjected to shortening once they had subsided deeply into the salt analog. The only difference between Models 1a and 1b was that in Model 1a minibasins 3 and 6 were sunk deeper in our salt analog before regional shortening was applied to the system (see details in Fig. 5). The goal of these two models was to test the impact of minibasin depth, and welding, on initial minibasin mobility. Primary and secondary welding also occurred in this model set and we document the impact of these processes on minibasin mobility and tilting. Note that the salt analog in Models 1a and 1b abruptly terminates east of the minibasin array and thus contractional thickening of our salt analog occurred at this side of the rig during shortening. In nature this could represent the actual edge of the salt basin, or a transition to more marginal, less mobile evaporites. Model 2 tested the impact of a plunging base-of-salt high block on minibasin mobility and tilting (Fig. 5). The base-of-salt high block was built using the same granular materials as our minibasin infills and the salt analog was deposited atop, and on either side of, this high block (Fig. 5). And finally, Model 3 tested the impact of an array of intrasalt minibasins on salt flow and suprasalt minibasin translation, secondary welding, and rotation during regional shortening (Fig. 5). When compared to the models of Rowan and Vendeville (2006), our models contain a higher proportion of salt such that minibasins are fully-surrounded by salt. As such, our minibasins are neither connected to one another by roof stratigraphy or welded to the base-salt prior to the onset of shortening (unless otherwise stated) (Fig. 5).

4 Minibasin Translation During Shortening

Why do minibasins translate during regional shortening? The fundamental process driving minibasin translation during regional shortening is captured in the results from Model 1a (setup shown in Fig. 5). As the moving endwall shortens the initial configuration, the weak polymer (our salt analog that we herein refer to as ‘salt’ for simplicity) preferentially absorbs the shortening strain and flows eastwards towards the foreland, expelling from between the minibasins, and thickening vertically in the absence of a mechanically-significant roof (Fig. 6) (see physical modelling movies in Dooley, 2020). Critically, this eastward-flowing salt pushes against the western flank of each of the minibasins, propelling them eastwards (Fig. 6). In contrast to the salt, the largely constant displacement magnitudes within the minibasins (color indicating the shortening-parallel (eastwards) displacement of the top model surface is broadly consistent across each minibasin on Fig. 6a and b) indicate that the relatively strong minibasins translate with the flowing salt and do not deform internally. Furthermore, as salt thickens vertically around the minibasins as the system shortens, we suggest that in natural shortened basins where the initial salt basin area is unknown, minibasin thickness cannot be used as a proxy for original salt thickness.

What controls how far and how fast a minibasin translates during shortening? At the largest scale, a major control on minibasin translation is the direction of strain propagation. Results from Model 1a show shortening propagates eastwards through the system, as indicated by the greater displacement of salt near the moving western endwall (Fig. 6). The eastwards decrease in salt flow magnitude means minibasins closer to the moving endwall are propelled more-strongly by flowing salt and thus translate at higher velocities (orange and green colored minibasins) than those further east (purple and blue colored minibasins) (Fig. 6). Model 1a results also suggest that the velocity of translation of every minibasin decreases as cumulative shortening increases (the color of each minibasin in Fig 6a indicates a higher horizontal velocity than the color of the correponding minibasin in Fig 6b). We explain this by the fact that sediments were continually added to the minibasins during regional shortening and thus they thickened during shortening. The result being that the thickness of salt beneath each of the minibasins decreased during regional shortening, with the resulting increased friction or viscous drag lowering the translation velocity of the salt, and hence also reducing the translation velocity of the minibasins (*cf*. 6a and 6b; *sensu* Wagner III and Jackson, 2011; Fernandez et al, 2020b).

Local-scale variations in salt flow velocity can also influence how far and how fast minibasins translate during regional shortening. We can explore this in Model 1a, where as salt near the moving endwall flows eastward, it encounters the thicker Minibasin 3 that was close to being welded to the base-salt at the onset of shortening (Fig. 6a). This minibasin does not translate basinwards as fast as the salt to its west (SMB3 has lower shortening-parallel [eastwards] displacements [light-green color] than the salt [orange color]), and it thus forms a barrier to the eastward-flowing salt. Eastward-flowing salt diverts around Minibasin 3, being funnelled into two fast-flowing salt streams (Fig. 6a) (*sensu* Talbot and Pohjola, 2009), one to the north and one to the south (labelled A and B on Fig. 6a). The salt stream to the north (A) is more strongly-developed and is faster-flowing than that in the south (B), most likely due to the wider gap (and thus greater salt flux) between Minibasins 1 and 3 than between Minibasins 2 and 3 (Fig. 6a). The salt streams continue eastwards towards the thinner, unwelded Minibasins 4 and 5, minibasins that were initially located approximately the same distance from the western endwall (Fig. 5). The faster-flowing salt stream behind Minibasin 4 explains why this minibasin is strongly-propelled and translates further eastwards (light-green color) than weakly-propelled Minibasin 5 (dark green to black color) (Fig. 6a). These observations suggest that how far and how fast an unwelded and otherwise unimpeded minibasin may translate during regional shortening is governed largely by the horizontal velocity of the salt stream that is propelling it. Fundamentally, the horizontal velocity of a salt stream is controlled by proximity to the moving endwall (a proxy for the orogenic hinterland), and the geometry of the salt flow pathways. Thus, the distribution of minibasins, their thicknesses, and the sizes of gaps between them are fundamental controls on minibasin mobility.

Translating minibasins driven by flowing salt can be impeded in a number of ways. The most obvious one is due to primary welding, but they can also be impeded by collisions with positive base-salt relief or intrasalt bodies. Evidence of translating minibasins being impeded by primary welds is shown in Model 1b where, prior to the onset of regional shortening, Minibasins 1 and 2 were both located the same distance from the moving endwall (Figs. 5 and 7). Minibasin 1 welded to the base-salt earlier than Minibasin 2 (as determined by a timelapse underside view of the model, and the sheared primary weld visible beneath Minibasin 1 in Figure 7). Primary welding preferentially restricts the eastward motion of Minibasin 1, resulting in a significant deficit in translation during shortening relative to Minibasin 2 (Fig. 7). These observations suggest that as a minibasin welds to the base-salt, the increase in friction or viscous drag at the interface may partially or fully impede minibasin translation.

Minibasin translation may also be impeded when minibasins collide with positive base-salt relief (or with other minibasins that are already buttressed). We examine this in Model 2, which simulates the buttressing effect of a plunging base-salt structural high on a linear array of minibasins (model setup outlined in Figure 5) (see also Jackson et al., 2020). As the moving endwall shortens the initial configuration and the salt is displaced eastwards, the minibasins are also mobilized, but are gradually buttressed by the plunging base-salt high. Minibasin 1, located adjacent to the tallest portion of the base-salt high block, translates a much shorter distance than

Minibasin 3, which lies adjacent to the lowest portion of the base-salt high (Fig. 8a-c). Thus, the greater the height overlap between the base of the minibasin and the top of the base-salt high block, the more efficient the buttress is.

The presence of intrasalt sediment bodies (or encased minibasins) between suprasalt minibasins may impede minibasin translation in a similar way to positive base-salt relief. We explore this in Model 3, which initially consisted of a series of intrasalt and suprasalt minibasins (see model setup in Fig. 5). As the moving endwall shortens this system, salt flow propels the shallower western suprasalt minibasins towards the eastern suprasalt minibasins and intrasalt minibasins. Where intrasalt minibasins are located directly between the converging suprasalt minibasins they act as buttresses, propping apart and preventing collision and secondary welding of the suprasalt minibasins (Fig. 9). Duffy et al. (2017) propose a similar situation occurred in the SE Precaspian Basin (Kazakhstan).

5 Minibasin Tilting During Shortening

Entire supra-salt and encased minibasins can tilt, that is, rotate around a horizontal axis. Some of the major causes of minibasin tilting include: i) regional shortening (e.g. Hudec et al., 2009; Lopez-Mir et al., 2014; Kergaravat et al., 2016; 2017; Ribes et al., 2017; Granado et al., 2018, Legeay et al., 2019); ii) asymmetric subsidence above salt of varying thickness (Jackson et al., 2020); iii) progradational loading (Ge et al., 1997; Callot et al., 2016) iv) pivoting of minibasins after primary welding (e.g. Rowan and Weimer, 1998; Callot et al., 2016; Ge et al., 2019); and v) kinematic interactions between subsiding minibasins (Fernandez et al., 2020c). For non-encased minibasins, syn-depositional tilting phases are recorded by the deposition of wedge-shaped growth packages (e.g. Rowan and Weimer, 1998, Jackson et al., 2020; Fernandez et al., 2020c), whereas post-encasement tilting of minibasins occurs entirely within the salt and is thus not expressed stratigraphically in the minibasins themselves (Callot et al. 2016; Duffy et al., 2017; Fernandez et al. 2017). In this section our physical models show how minibasin tilts are highly spatially- and temporally-variable during regional shortening. We outline what key factors may influence minibasin tilting during regional shortening, addressing in particular the influence of pressurized salt and minibasin interactions with base-salt relief or other minibasins.

At an early stage of regional shortening of Model 1b, five out of the six minibasins tilt broadly or directly towards the west, whereas Minibasin 5 tilts roughly towards the north (Fig. 10a). A cross-section from Model 1b taken through Minibasins 2, 3 and 4 at the end of shortening (of 33 cm) also shows consistent tilting of lower minibasin packages towards the west (Fig. 11a). This consistent early tilt towards the moving endwall occurs prior to welding of any of the six minibasins to the base-salt or to one another, in this case ruling out minibasin collision or welding to base-salt as potential contributing factors during the early stages of shortening (Fig. 10a). We suggest that this consistent westward tilt direction is likely a function of the moving endwall continually pumping salt eastward, a process that pressurizes salt at the eastern end of the salt basin (Fig. 10a). Thus, we postulate that during this phase, minibasins tilt westwards, away from zones of pressurized salt on their eastern flanks within the salt basin (*sensu* Hudec et al., 2009; Fernandez et al., 2020c) (Fig. 10a). Evidence for extreme pressurization of the salt on the eastern side of the salt basin is present in an arbitrary line through suprasalt minibasins 5 and 6 in Model 1b (Fig. 11b). Here we see that Minibasin 5 contains a thick package of synshortening sediments overlying the initial bowl-shaped package (Fig. 11b). In contrast, Minibasin 6, located close to the eastern margin of the salt basin, exhibits a similar-thickness bowl-shaped fill overlain by a condensed synshortening sequence, and underlain by thick salt (Fig. 11b). Furthermore, the base of Minibasin 6 lies almost at the original top-salt level, indicating that this minibasin, even though denser than the model salt, was buoyed up by the pressurized salt caused by continuous pumping of model salt eastwards during shortening (Fig. 11b).

Minibasins in Model 1b change tilt direction as regional shortening strain increases (Fig. 10). An example is Minibasin 1, a minibasin that was not welded to the base-salt at the onset of shortening and does not collide with any other minibasins during shortening (Fig. 10). At relatively low regional shortening strains, Minibasin 1 tilts broadly towards the moving western endwall (WNW in Fig. 10a), then displays a horizontal top surface (Fig. 10b), before eventually tilting towards the northeast at a higher regional shortening strain (Fig. 10c). Given the isolated nature of Minibasin 1 we suggest the likeliest causes of the changes in tilt direction are: i) the initially WNW-tilting Minibasin 1 welded to the base-salt at some point after the onset of shortening and pivoted on the primary weld (*sensu* Rowan and Weimer, 1998; Callot et al., 2016; Ge et al., 2019; Fernandez et al., 2020c), with the centre of mass, geometry of the primary weld, and minibasin shape favouring late-stage tilt towards the northeast; and/or ii) regional shortening and relative changes in the location and horizontal translation velocities of minibasins resulted in shifts in the location of pressurized salt around the minibasin through time, with the minibasin tilting away from these zones (*sensu* Hudec et al., 2009; Fernandez et al., 2020c). Controls such as these are likely to be significant for any minibasin, particularly those that do not collide with other minibasins, and are likely to vary during the evolution of the system.

Minibasin tilt directions also change significantly after they collide with other minibasins (e.g. Minibasins 2 and 3, as well as Minibasins 5 and 6 in Model 1b; Fig. 10). For example, the tilt direction of Minibasin 5 changes by almost 180° from a stage prior, but close, to the onset of collision with Minibasin 6 (Fig. 10a), to a late stage in the collision process (Fig. 10c). We also see that at an early stage in its collision with Minibasin 3, Minibasin 2 tilts southeast (Fig. 10b), whereas later in the collision process it tilts northeast (Fig 10c). We speculate that when minibasins collide, in addition to the potential for changes in tilt direction and magnitude due to pivoting on primary welds or tilting away from zones of pressurized salt outlined above, the following factors may influence minibasin tilt histories: i) whether collision was 'head on' or 'glancing' and thus the potential for minibasins to slide past, or pivot and rotate (around a vertical axis) against one another; ii) the relative horizontal translation velocities of the minibasins; iii) the relative sizes of the minibasins; iv) the thickness of salt underlying the minibasins prior to collision; and v) changes in the location of salt streams and pressurized salt through time.

Model 2 explores how the direction and magnitude of minibasin tilting during regional shortening may be influenced by base-salt relief. Height-change maps illustrate how minibasins tilt away from the southward plunging high block during simple vertical loading as well as during regional shortening (Fig. 8b and c). Cross-sections of Model 2 taken through Minibasins 1, 2 and 3 at the end of regional shortening show that each minibasin initially developed a symmetrical bowl-shaped package that is overlain by a wedge-shaped package that thickens away from the plunging high block (Fig. 8c). We interpret that minibasins tilt away from the plunging high due to the higher rate of salt flow from beneath the western flanks of the minibasins when compared to flow from beneath the eastern flanks (Fig. 8). This is a result of salt flow beneath the eastern flanks of the minibasins being perturbed and restricted by the plunging base-salt high creating zones of pressurized salt, with minibasins tilting westwards, away from these zones (*sensu* Hudec et al., 2009; Fernandez et al., 2020c; Jackson et al., 2020; Fig. 8). The transition from bowl- to wedge-shaped packages in cross-section thus marks the onset of asymmetrical salt flow from beneath the minibasins during the vertical loading stage as the subsiding minibasin was more impacted by the base-salt high block (Fig. 8b-c). Notably, during vertical loading, the amount of westward minibasin tilt was greater where the plunging base-salt high block was taller (compare the subsidence maps of Minibasin 1 and Minibasin 3 in the 'vertical subsidence' stage in Fig. 8b). This suggests, intuitively, that the taller the base-salt feature, the more it forms a barrier to salt flow, resulting in more strongly developed pressurized salt zones and greater amounts of tilt away from them. During regional shortening the overall tilting effect was enhanced as the minibasins were pushed up against, and onto, the base-salt high block (Fig. 8). However, cross-sections show that after regional shortening, the top of layer 3 of the minibasin fill was tilted 17° for Minibasin 3, yet only 10° for Minibasin 1 (Fig. 8c), reversing the patterns seen during the vertical subsidence stage (Fig. 8b). Given that Minibasin 3 was initially located adjacent to a lower-relief base-salt high than Minibasin 1, we can surmise this factor governed enhanced tilting during shortening (Fig. 8b and c). Where the structural relief was higher, in the north of Model 2, minibasins were buttressed against the step at base of salt, preventing further translation and associated tilting. The lower structural relief in the south of the model allowed Minibasin 3 to translate further eastwards (3.5 cm more than Minibasin 1, Fig. 8c), up and onto, the base-salt high during shortening. Continued eastwards translation was accompanied by enhanced tilting as Minibasin 3 continued to move up onto the lower-relief base-salt step (Figs. 8b and c).

Overall, for minibasins surrounded by salt (i.e. not welded to the base-salt or colliding with other minibasins), tilt changes are likely driven by changes in the locations of pressurized salt, a factor which may be modified by shortening-induced salt flow or effects of base-salt relief (*sensu* Hudec et al., 2009; Jackson et al., 2020; Fernandez et al., 2020c). Once minibasins weld to the base-salt or collide with other minibasins, pivoting on primary and secondary welds becomes significant.

6 Minibasin Rotation During Shortening

Model 3 shows that minibasins can rotate around vertical axes during regional shortening (Figs 5 and 12) (see physical modelling movies in Dooley, 2020). Strikingly, all suprasalt minibasins in Model 3 rotate significantly, with a component of rotation occurring before suprasalt minibasins welded to the base-salt (or edge of salt) or collided with other minibasins, and a component of rotation occurring afterwards (Figs. 12-14). So, why do minibasins rotate prior to welding? A likely cause of rotation is evident in Figures 13 and 14a, as SMBs 1, 3 and 5 underwent the majority of their rotation prior to welding. In these figures salt streams are developed in the deepest portion of the salt (and thus detected by the DIC technique). These streams vary markedly in extent and horizontal velocity, with the differences likely related to the relative rates of flux of salt between the western proximal suprasalt minibasins and/or the edge of salt (Figs. 13 and 14a). We propose that differences in the horizontal velocities of salt streams exert different degrees of traction on different parts of the minibasin margins. This will generate asymmetric viscous drag or shear on minibasin margins and promote their rotation (Figs. 13 and 14a). This concept is best-illustrated, albeit simplistically, by suprasalt Minibasin 1, which has a slower-moving salt stream between itself and the edge of salt to its north, and a faster moving salt stream between itself and suprasalt Minibasin 3 (Fig. 14a). These differences in the horizontal velocities of salt streams to the north and south of suprasalt Minibasin 1 generate viscous drag or shear on the minibasin boundary, driving anticlockwise rotation of suprasalt Minibasin 1 (Fig. 14a). However, such logic does not apply to some of the other suprasalt minibasins (e.g. suprasalt Minibasin 3 in Figs. 13 and 14, which rotates towards what appears to be a larger and faster-flowing salt stream to its north). We suggest this is a function of the 3-D nature of both salt flow and the outer surfaces of the minibasins, as well as limitations of our experimental monitoring. Notably, the salt streams captured on the underside of the model by the digital image correlation (DIC) technology (Figs. 13 and 14) are processed entirely in 2D and may only be showing flow patterns in the deepest portion of the salt, or capturing only portions of the velocity fields defined by marker plugs within our model salt. In reality, however, these flows will vary upwards in width and horizontal velocity due to upwards changes in: i) geometry of the minibasins and thus width of the stream; and ii) the relative effect of viscous drag from the top and base of the salt, and from the wallrock (minibasin flanks) as these gaps narrow during shortening and secondary welding. To accurately constrain the viscous drag or shear imparted on a minibasin and test the differential traction exerted by salt streams on the resulting minibasin rotation we need a high resolution map of the 3-D distribution of traction exerted on the outer surface of the minibasin. We do not have this data available. However, we believe the concept outlined here provides the basis for testing in future physics-based numerical models.

Minibasins also rotate after welding to the base of salt, or as they collide and pivot against other minibasins, or against the edge of salt. The influence of base-salt welding is shown in Model 3, as Minibasins 2, 4 and 6 were welded to the base-salt prior to the onset of shortening (Fig. 5). Only at advanced stages of regional shortening do these minibasins rotate (Figs 12b, 14b and Model 3 Underside Full.mov, and Model 3 Underside_Vectors and Displacement.wmv in Dooley et al., 2020). Interestingly, the axis of rotation of each of these minibasins is not located below the minibasin centre, instead it is located towards the southern margin (Figs. 12b and 14b). We propose that these minibasins rotated due to a combination of eastward-advancing salt streams and their convergence along with the minibasins pivoting on base-salt welds. The off-centre location of the axis of rotation of Minibasins 2, 4 and 6 is controlled by where these minibasins welded most strongly to the base-salt (the pivot point), which is, in turn, influenced by how each of the minibasins tilted (Model 3 Underside Full.mov in Dooley et al., 2020). The influence of minibasin collisions with one another and/or the edge of salt on minibasin rotation are also seen at intermediate-to-high regional shortening strains in Model 3 (Fig. 14; Dooley et al., 2020). A good example is intrasalt Minibasin 5, which prior to regional shortening was welded to the base-salt and also located relatively close to the southern edge of salt (Figs. 5 and 12; Dooley et al., 2020). As regional shortening ensues, suprasalt Minibasin 5 translates eastward and collides with the northwestern portion of intrasalt Minibasin 5 (see Model 3 Underside Full.mov in Dooley et al., 2020). This off-centre collision and continued eastward translation of suprasalt Minibasin 5, possibly in combination with intrasalt Minibasin 5 becoming pinned to the southern edge of the salt, facilitates significant clockwise rotation of intrasalt Minibasin 5 as it is pushed eastwards (46° clockwise rotation after 31 cm of regional shortening in Fig. 12b; see Model 3 Underside Full.mov in Dooley et al., 2020). We suggest that the direction, amount and speed at which minibasins rotate after collision is controlled by factors that include: i) the angle and force of collision; ii) the morphology of minibasin collision surfaces; iii) the presence, location and extent of primary welds; iv) the direction and speed of any rotation occurring prior to collision; v) the number of minibasins involved; and vi) whether a minibasin is pinned against the edge of salt. We also expect that the effect of differences in the horizontal velocity of salt streams will also exert viscous drag or shear on minibasin surfaces and promote minibasin rotation even after primary welding or collision with another minibasin. We suggest that many of the factors outlined here apply and influence minibasin rotation when large-scale supra-salt minibasins collide in nature (e.g. Rowan and Vendeville, 2006). These influences are summarized in Figure 15.

7 Discussion

7.1. Conceptual Models of Shortening in Isolated-Minibasin Provinces

Based on observations from our physical models and existing literature, we now present 3D conceptual models that summarise how, why and where many of the key processes and structural styles occur as an isolated-minibasin province shortens (Fig. 16). As in our physical models, these conceptual models focus on the thin-skinned component of regional shortening, with shortening propagating from the hinterland on the left. We assume the increased rate of salt rise due to regional shortening is balanced by the rate of syn-kinematic sedimentation and erosion of the minibasins, such that the top model surface remains essentially flat and no salt canopies, encased minibasins, or diapir roofs form (other model assumptions are noted in figure caption).

Prior to regional shortening, minibasin subsidence was largely symmetrical, being dominated by bowl-shaped stratigraphic units (blue in Fig. 16a). The exception is Minibasin 7, which shows a wedge-shaped unit that represents a phase of asymmetrical subsidence developed as the minibasin tilted away from the underlying base-salt high and towards the thicker salt in its foreland (Fig. 16a) (*sensu* Jackson et al., 2020). The only driver of salt flow prior to regional shortening is therefore differential vertical subsidence of the minibasins.

At low regional shortening strains, shortening-induced regional salt flow pushes against minibasin margins and propels them towards the foreland, with translation of minibasins closer to the hinterland generally initiated before those in the foreland (Fig. 16b). Salt streams of locally high horizontal salt flow velocity form where salt flows through the relatively narrow gaps between minibasins. High degrees of minibasin translation are expected ahead of those streams. The net effect of these processes is that minibasins converge and the intervening salt thickens vertically (diapir rise). In some cases, such as near the hinterland, minibasins collide, unless propped apart by base-salt relief or encased minibasins; Duffy et al. (2017) document such a buttressing effect of encased minibasins in the SE Precaspian Basin (Kazakhstan). Early stages of regional shortening may see minibasins preferentially tilt towards the hinterland (away from the zone of pressurized salt situated towards the foreland; *sensu* Fernandez et al., 2020c), although these tilts may be modified by interactions with base-salt relief or adjacent minibasins. At low regional shortening strains, many salt walls remain open, particularly those aligned broadly parallel to the regional shortening direction, and those furthest from the hinterland; as a result, many salt flow pathways remain open (Fig. 16b). Viscous drag or shearing imparted by variations in the horizontal velocity and direction of salt streams is therefore a likely cause of minibasin rotation, along with pivoting on any primary and secondary welds. Some minibasins may horizontally translate, tilt and rotate simultaneously (e.g. Minibasin 4 in Fig. 16b).

At high regional shortening strains, most minibasins will have collided with one or more adjacent minibasins resulting in a complex map-view distribution of secondary welds, thrusts and subvertical shear zones (with components of strike-slip, reverse, and normal displacement possible) (Fig. 16c; see also Rowan and Vendeville, 2006). Minibasins welded to the base-salt at lower regional shortening strains continue to translate, shearing the primary welds. If the regional shortening strains and induced salt flow are sufficient, some minibasins aligned in the regional shortening direction and that shared a secondary weld, may translate as a single body, such as that seen in our Model 1b (Figure 11; Dooley et al., 2020). Secondary welds oriented broadly perpendicular to the regional shortening direction can transform into thrust welds, whereas secondary welds oriented oblique to the regional shortening direction can transform into thrusted welds with a component of strike-slip (Fig. 16c; *sensu* Jahani et al., 2017; Hassanpour et al., 2018). These welds, in combination with the buttressing effects of base-salt relief, drive extreme minibasin tilting. In general, minibasin tilt directions are likely largely governed by the angle of contact and relative force of minibasin collisions, with primary welds acting as pivoting surfaces. In contrast to the lower strain stage of regional shortening, the dominant driver of rotation is the relative angle and force of minibasin collisions.

7.2. Influence of Pre-Shortening Salt Volume and Distribution on How Salt Basins Shorten

We now synthesise how variations in pre-shortening salt volume and distribution can influence how salt basins shorten (Fig. 17). Of particular interest here are the striking differences between shortened isolated-diapir and shortened isolated-minibasin provinces (*cf*. this paper and Duffy et al., 2018). Of these initial configurations that contain diapirs prior to the onset of regional shortening, isolated-minibasin provinces will typically contain the highest volume of salt prior to regional shortening. Due to the weak nature of salt, the configuration with the highest salt volume, and where salt fully surrounds minibasins, typically results in a system with: i) the lowest mechanical rigidity; ii) the most independently-mobile minibasins; and iii) overall, a different shortening style to isolated-diapir systems (Fig. 17b and c).

One of the distinguishing characteristics of isolated-minibasin systems is that even at moderate regional shortening strains, shortening is cryptic, being accommodated by salt flow and vertical thickening (Fig. 17c). As such, unless a roof records any deformation, as is the case in the SE Precaspian Basin (Duffy et al., 2017), detecting regional shortening or unravelling the original pre-shortening configuration of minibasins is more difficult than in squeezed isolated-diapir systems, where the surrounding sediments visibly shorten (Fig. 17c; e.g. Callot et al., 2007; Dooley et al., 2009). Detecting shortening at higher regional shortening strains is possible as minibasins collide, may over- and under-thrust one another, and give rise to degrees of minibasin tilt and rotation (e.g. Duffy et al., 2017; Legeay et al., 2019; Figure 16c). A second difference is that during regional shortening of isolated-minibasin provinces, deformation is accommodated either by salt flow and vertical thickening, or one of a combination of translation, tilt (in a variety of directions), or rotation of entire minibasins (Fig. 17c). Minibasins, although dynamic and interacting with other minibasins, may thus remain largely internally-undeformed, as in the SE Precaspian Basin, a characteristic that is uncommon in shortened isolated-diapir systems (Fig. 17b; *cf*. Gottschalk et al., 2004; Callot et al., 2007; Dooley et al., 2009; Kergaravat et al., 2016; 2017; Duffy et al., 2017, 2018; Ribes et al., 2017; Granado et al., 2018; Legeay et al., 2019). A third difference is that thrust axes and secondary welds do not form relatively continuous trends oriented broadly perpendicular (with some deviations, as outlined by Jahani et al., 2017 and Hassanpour et al., 2018) to the regional shortening direction as is typical of shortened isolated-diapir provinces (e.g. Fars Province of Zagros fold-and-thrust belt [e.g. Callot et al., 2007; Jahani et al., 2009]) or even shortened areas of undeformed salt (e.g. Jura Mountains [e.g. Laubscher, 1961]). Instead, the orientations and extents of thrust axes and secondary welds are highly-variable, being controlled by the shape and disposition of the minibasins and how they have fitted together (Figs. 16 and 17).

7.3. Complex Patterns in Natural Shortened Salt Basins

The pre-shortening salt volumes and configurations we have described (undeformed salt, isolated-diapir, and isolated-minibasin), represent schematic end-member scenarios intended to aid understanding of the different mechanical behaviors that govern how salt basins shorten (see companion paper by Duffy et al., 2018). We stress that many natural shortened salt basins that developed where the pre-existing salt contained diapirs, may lie on the continuum between isolated-minibasin and isolated-diapir scenarios, showing elements of shortening styles associated with both. A good example is the egg-carton-like precursor salt geometry common in the sub-canopy system of the northern Gulf of Mexico (e.g. Rowan and Vendeville, 2006). Here, isolated diapirs were connected at depth by salt anticlines that radiated out, and plunged away from the diapirs, forming a polygonal network (Rowan and Vendeville, 2006). When shortened, the system behaved partly as a relatively mechanically-rigid isolated-diapir system, with: i) salt predominantly extruded from the tallest diapirs located at ridge junctions; and ii) variations in shortening styles between diapirs at ridge junctions and above the more deeply-buried ridges (Rowan and Vendeville, 2006). However, the system also displays elements that suggest it behaved partly as an isolated-minibasin system, with regional shortening focused on a polygonal diapir network and evidence of independently-mobile and rotated minibasins (Rowan and Vendeville, 2006).

When applying the concepts outlined in this paper and Duffy et al. (2018) to natural examples, it is important to note that the volume and distribution of pre-shortening salt that influenced a basin during regional shortening may vary spatially and temporally. For example, the Sivas Basin, Turkey is interpreted to have had thinner, undeformed salt in its Western Domain based on the presence of a simple fold-and-thrust belt characterised by linear folds and thrusts striking perpendicular to the regional shortening direction (Kergaravat et al., 2016; Legeay et al., 2019). In contrast, its Central Domain contains many tightly-packed, welded minibasins, some with extreme tilts, and thus consisted of isolated minibasins prior to regional shortening (Fig. 4c and d) (Kergaravat et al., 2016; Legeay et al., 2019).

A second example is the sub-canopy region of the salt-stock-canopy province in the lower-slope of the northern Gulf of Mexico. This area has experienced protracted regional shortening in the contractional domain of a gravity-driven passive margin system detached on the autochthonous Louann salt (e.g. Diegel et al., 1995; Peel et al., 1995; Rowan et al., 1999; Pilcher et al., 2011; Dooley et al., 2013). Fiduk et al (2016) (their Figure 4) present a regional base salt canopy map that shows isolated diapirs surrounded by a rigid, continuous sediment body, that is, an isolated-diapir scenario, in the central-southern region. In contrast, in the northeast, more diapirs are present in the form of partially-connected linear salt walls. This configuration is a hybrid of the isolated-minibasin and isolated-diapir scenarios. Thus, different parts of the same basin contain different salt volumes and distributions, a factor that may result in different mechanical responses to lateral regional shortening, and different structural styles.

Natural fold-and-thrust belts may also contain multiple detachment levels as a result of canopy development (e.g. Sivas Basin, Turkey [e.g. Ringenbach et al., 2013; Callot et al., 2014; Kergaravat et al., 2016; 2017; Ribes et al., 2017; Legeay et al., 2019]; northern Gulf of Mexico, USA [e.g. Diegel et al., 1995; Peel et al., 1995]; Axel-Heiberg Island, Artic Canada [Jackson and Harrison, 2006; Harrison and Jackson, 2014]; Betics in Southern Spain [Flinch and Soto, 2017]) or due to the occurrence of different weak (detachment) layers in the deformed section (e.g. Zagros fold-and-thrust belt, Iran [Sherkati and Letouzey, 2004; Verges et al., 2011; Najafi et al., 2014;

Ghanadian et al., 2017; Hassanpour et al., 2020]). Duffy et al (2020) show an example from the mid-lower slope region of the northern Gulf of Mexico (their Figure 4), where the sub-canopy consists of isolated feeders (isolated-diapir scenario). In contrast, above the canopy, isolated minibasins subside into the Sigsbee salt canopy (isolated-minibasin scenario). In such systems, regional shortening associated with different detachment levels may thus affect different precursor salt volumes and configurations, and shortening styles may vary significantly between deep and shallow systems. This concept is highlighted by the different shortening styles that occur for example above and below the allochthonous salt in the Betics (e.g. Flinch and Soto, 2017).

8 Summary

This study has used observations from natural shortened salt basins and a suite of new physical models to examine the processes and structural styles that occur in shortened isolated-minibasin provinces. Our key findings are:

- When regional shortening occurs, the weak salt localizes contractional strain and the strong, mobile minibasins initially move independently of one another. Regional shortening in isolated-minibasins provinces may therefore be hard to detect, particularly at low shortening strains, as regional shortening is primarily accommodated by salt thickening vertically (diapir rise). This means that minibasin thickness is not a proxy for original salt thickness in shortened isolated-minibasin provinces.

- As weak salt localizes contractional strain it induces salt flow, in some cases in highly-localized streams of high horizontal velocities. This flowing salt pushes against the hinterland-side of rigid minibasins, propelling them in the direction of regional shortening. Several factors can restrict the translation of minibasins during regional shortening: i) the presence of relatively thin salt below the minibasin; ii) friction associated with primary welding; and iii) collision and buttressing effects of base-salt relief, intrasalt bodies or intrasalt minibasins.

- Isolated minibasins commonly tilt during regional shortening (i.e. rotate around horizontal axes), with the direction and magnitude of tilt being highly spatially and temporally-variable. In our models, minibasins tend to tilt gently toward the hinterland at low strains, which we attribute here to being a result of differential salt pressure within the basin. A regionally-consistent tilt direction may therefore indicate regional shortening, but we propose that this tilt may commonly be modified or even reversed by: i) asymmetric subsidence associated with structure or relief at base salt; ii) pivoting on primary welds; iii) minibasin collision; and iv) tilt away from other localized zones of pressurized salt. Tilts can become extreme at high regional shortening strains, facilitated by minibasin collision, thrusted secondary welds, and the buttressing effect of base-salt relief.

- Minibasins can rotate around vertical axes to significant degrees during regional shortening. In the absence of welding and/or collision with other minibasins or base-salt relief, minibasin rotation is likely caused by viscous drag or shearing imparted on the minibasin boundary by variations in the horizontal velocity and direction of salt streams in 4D. Variations in horizontal flow velocities of streams are likely to develop as a result of the local geometry and configuration of minibasins (note that our minibasins are circular in map-view), the edges of the salt basin, and the local dip. Once minibasins weld to the base-salt, or collide with base-salt relief, intrasalt bodies or the edge of the salt basin, they may rotate as they jostle with and pivot against these features, likely aided by continued flow-induced shearing and/or viscous drag.

- The kinematics of minibasins in shortening isolated-minibasin systems may be complex and highly-variable both spatially and temporally. Minibasins may experience varying degrees and rates of translation, tilt and rotation; in some circumstances these processes may occur independently, but in others they may occur simultaneously. The extent to which the different processes affect a minibasin is likely dependent on factors that amongst others includes: tectonic boundary conditions; the size, geometry and spatial configuration of minibasins; the thickness of salt underlying minibasins; and the nature of local base-salt relief.

By placing the findings of this paper into context with those of companion paper Duffy et al (2018), we conclude that differences in the volume and distribution of salt prior to regional shortening result in different kinematic processes and structural styles. In particular, these processes and structural styles vary markedly between settings where pre-shortening salt is in flat-bedded, isolated-diapir, or isolated-minibasin end-member configurations, respectively. These end-member settings differ in terms of: i) thrust style and evolution; ii) map-view configuration of faults and welds; iii) degree of internal deformation within the minibasins; iv) minibasin mobility; and v) the degree to which shortening may be accommodated by cryptic deformation. We also note how natural shortened salt basins show evidence of having had initial salt volumes and distributions that were hybrids of the end-member configurations outlined in the pair of papers. Furthermore, basins may show spatial variations in pre-shortening salt volume and distribution, and this may also vary through time.

9 Acknowledgements

We would like to thank Nancy Cottington for figure drafting, along with Martin Jackson, Gillian Apps, Frank Peel, and Mark Rowan for scientific discussions. We also thank reviewers Jafar Hassanpour and Zhiyuan Ge, along with editor Craig Magee for their thorough and constructive reviews of this work. The project was funded by the Applied Geodynamics Laboratory (AGL) Industrial Associates program, comprising the following companies: Anadarko, Aramco Services, BHP Billiton, BP, CGG, Chevron, Condor, EcoPetrol, EMGS, ENI, ExxonMobil, Hess, Ion-GXT, Midland Valley, Murphy, Nexen USA, Noble, Petrobras, Petronas, PGS, Repsol, Rockfield, Shell, Spectrum, Equinor, Stone Energy, TGS, Total, WesternGeco, and Woodside (http://www.beg.utexas.edu/agl/sponsors). The authors received additional support from the Jackson School of Geosciences, The University of Texas at Austin. Publication authorised by the Director, Bureau of Economic Geology, The University of Texas at Austin. The authors confirm no conflicts of interest.

10 Data Availability Statement

The physical modelling movies that support the findings of this study are openly available in Figshare at: https://doi.org/10.6084/m9.figshare.12659828.v1

11 Figure Captions

Figure 1. Schematic diagrams showing a pre-shortening configuration typical of a) an 'isolated-diapir province' and b) an 'isolated-minibasin' province. In a) salt makes up a low proportion of the rock volume and is distributed in discrete salt stocks and walls. In b) salt makes up a higher proportion of the rock volume and forms a connected network of diapirs that surround isolated minibasins. The strength of any diapir roof stratigraphy is assumed to be negligible.

Figure 2. The style of shortening that occur in salt provinces is strongly influenced by whether or not diapirs were present prior to the onset of regional shortening. These forward models maintain salt area through time (after Hudec and Jackson, 2007).

Figure 3. Maps showing the top of salt (silicone polymer) at different stages of a physical modelling experiment into regional lateral shortening of a system where the pre-shortening salt distribution and volume was broadly analogous to an isolated-minibasin setting (Fig. 1b): (a) pre-shortening configuration and (b) after shortening. In a) minibasins are separated by a polygonal network of deep salt ridges, with shallow diapirs typically located at the ridge junctions. In the strictest sense, our definition of the isolated-minibasin end member, the deep salt ridges would be wider and would extend upwards to more fully-isolate each minibasin (see section 7.3). In b) diapirs and the ridges accommodate shortening and minibasins translate and interact with other minibasins. Redrawn and modified from Rowan and Vendeville (2006).

Figure 4. Map and section views showing general characteristics of some natural shortened isolated-minibasin provinces. (a) Structure map of the Top Kungurian Salt from a portion of the mildly-shortened SE Precaspian Basin (Kazakhstan). Structural lows host isolated minibasins that are surrounded by a polygonal network of diapirs (modified from Fernandez et al. [2017]). (b) geoseismic section taken along the kinked black and white line in a) that shows the main structural elements of the area. Note the tilting of the supra-salt minibasin fill (modified from Duffy et al. [2017]). c) Simplified geological map of the highly-shortened central portion of the Sivas Basin, Turkey, showing the distribution of minibasins (blue), salt (red), and key structural features. Note how minibasins are isolated from one another, being surrounded on all sides by salt or an equivalent weld. Map modified from Kergaravat et al. (2016) and incorporating key data from Kurtman (1973), Guezou et al. (1996), and Poisson et al. (1996). d) Cross-section along Line X-X' in c) (parallel to shortening direction) showing a tectonic wedge with thrusts in pre-salt strata, and two generations of supra-salt minibasins separated by an evaporite canopy or an equivalent tertiary? weld. Note: i) the marked variations in tilts of the minibasins, some are flat-lying whereas

others are highly-upturned; and ii) the tight-packing of internally-undeformed minibasins. Pairs of black dots mark welds. Modified from Kergaravat et al. (2016) to include stratigraphic ages from Legeay et al. (2019).

Figure 5. Chart summarizing the design and parameters used for the physical models presented in the text. Models are numbered in the order they are introduced in the text. SMB = suprsasalt minibasin. IMB = intrasalt minibasin. All models have a North arrow as it allows simple description of model results around a frame of reference.

Figure 6. Maps showing the shortening-parallel (eastward) displacement on the top surface of Model 1a (calculated over a period of one minibasin sand fill cycle) at: a) 4.5 cm cumulative shortening; and b) 16.5 cm cumulative shortening. Warmer colours illustrate more eastward movement. A and B are salt streams that are flowing eastwards and propelling the eastward translation of Minibasins 4 and 5 respectively.

Figure 7. Underside view of Model 1b at the end of regional shortening (33 cm). Minibasin 1, which welded to the base salt earlier than Minibasin 2 has translated a shorter distance eastwards indicating that primary welding impedes minibasin translation. The yellow line shows the line of section of the SW-NE-oriented cross-section shown in Figure 11.

Figure 8. Outputs from Model 2. a) on left is the overhead view at the start of the model run and on the bottom is a schematic view of the degree of overlap between the base of the minibasins and the top of the plunging high prior to the onset of regional lateral shortening. On the right is an overhead view during shortening showing the shortening-parallel (eastward) displacement on the top surface of Model 2 (calculated over a period of one minibasin sand fill cycle). Warmer colours represent faster eastward-moving salt streams. b) views of the height change of top salt surface during the vertical subsidence stage (left) and during regional shortening (right). Note the marked tilt of minibasins towards the moving endwall (west) in both stages. c) W-E-oriented cross-sections through each minibasin at the end of shortening. Note the westward-thickening growth wedges and the tilting of the lower section of the minibasins towards the west. All minibasins have translated eastwards and welded onto the plunging high. Minibasins located adjacent to where the top of the plunging high is deeper (i.e. less of a barrier) translate further eastwards.

Figure 9. Outputs from Model 3. a) cross-section views at the end of shortening (location of sections shown in (b)), and b) underside view of Model 3 at end of shortening. Where one or more intrasalt minibasins (IMB's) are located directly between the converging suprasalt minibasins (SMB's) they act as buttresses, propping apart and preventing collision and secondary welding of the suprasalt minibasins.

Figure 10. Overhead views showing height change maps (calculated over a period of one minibasin sand fill cycle) that illustrate the translation and tilt changes that occur as Model 1b shortens at: a) 4.5 cm shortening, b) 19 cm shortening, and c). 23 cm shortening. Note the collision of minibasins and the marked spatial and temporal variation in tilt magnitude and direction as the model shortens.

Figure 11. a) SW-NE-oriented cross-section taken through supra-salt minibasins 2, 3 and 4 (oblique to shortening) at the end of shortening of Model 1b. Growth wedges immediately above the first blue unit indicate consistent early tilt of minibasins broadly towards the moving endwall. Location of section shown by yellow line on Fig 7, and white dashed line on Fig. 10. b) SW-NE-oriented cross-section taken through supra-salt minibasins 5 and 6 (oblique to shortening) at the end of shortening of Model 1b. Note the base of SMB6 lies near the original top of salt and the condensed synshortening sequence above SMB6 relative to SMB5. These observations indicate early uplift of SMB6, which we propose was driven by continuous pumping of model salt eastwards during shortening, which pressurized salt at the eastern end of the model. Location of section shown by white dashed line on Fig. 10.

Figure 12. Underside views of Model 3 at a) 16 cm (intermediate regional shortening strain) and b) 31 cm shortening (high regional shortening strain). a) Suprasalt minibasins 1, 3 and 5 rotate prior to forming primary or secondary welds. b) Minibasins can also rotate after forming primary or secondary welds, pivoting on the welds (or possibly the edge of the salt basin), with the axis of rotation being either in the centre of the minibasin or towards the margin. Intrasalt minibasins can prevent the collision of suprasalt minibasins during regional shortening.

Figure 13. Underside views of Model 3 at early stages of regional shortening showing the shortening-parallel (eastward) displacement at the model base (calculated over a period of one minibasin sand fill cycle). Note the gradual anticlockwise rotation of SMB 3. Small white arrows are vectors of movement and indicate rotation. Note the development of salt streams between the minibasins.

Figure 14. Underside views of Model 3 showing the shortening-parallel (eastward) displacement at the model base at: a) 8 cm shortening, and b) 17 cm shortening. Vector arrows indicate rotation of minibasins. Some rotations occurred before minibasins welded to the base salt formed secondary welds (e.g. SMB 3) or, and some occurred afterwards.

Figure 15. Map-view schematic model showing: i) some of the key drivers of minibasin rotation; and ii) some common interactions between supra-salt and intra-salt minibasins, that occur as an isolated-minibasin provinces shortens. Rotations around vertical axes are driven by variations in the magnitude, horizontal velocity and direction of salt flow as a result of: i) the local configuration of minibasins and intra-salt bodies; and ii) pivoting against other minibasins, base-salt relief or the edge of salt. Red = mobile salt. Grey = non-salt, immobile rocks.

Figure 16. 3-D conceptual block models synthesising the structural styles and processes that occur in isolated-minibasin provinces as they shorten. a) pre-shortening configuration. b) low regional shortening strain. c) high regional shortening strain. Salt is shown in red. The model is based on a system with a single generation of minibasins, with no salt canopies, and, with the exception of a single base-salt high, the base-salt is flat. We assume minibasins are largely unwelded to the base-salt prior to shortening, but as shortening ensues more minibasins ground to form primary welds – a scenario that ensures the widest range of structural styles and processes are captured in the conceptual model. We also assume flow perturbations related to minibasin subsidence were of insufficient scale to modify the subsidence patterns of adjacent minibasins (*cf.* Fernandez et al., 2020c).

Figure 17. Schematic comparison of the key characteristics of fold-and-thrust-belts developed with different precursor volumes and and distributions of salt: a) flat, undeformed salt; b) an isolated-diapir scenario (*sensu* Duffy et al., 2018); and c) an isolated-minibasin scenario (this paper). a) shows a relatively simple set of folds and thrusts striking perpendicular to the shortening direction and that are continuous along-strike. b) weak diapirs localize contractional strain and are squeezed. Faults and folds nucleate at diapirs, propagate out into the surrounding sedimentary rocks and link with those from adjacent diapirs. Folds and thrusts are not continuous along-strike, instead they deviate to link up precursor diapirs. There are marked along-strike variations in structural style; welds, squeezed diapirs and thrusted welds at diapirs, compared to folds and thrusts in the intervening sedimentary rocks. c) minibasins are independently-mobile and experience translation, tilting and rotation as they are propelled by flowing salt during shorteninig and collide with one another. Folds and thrusts may be highly-discontinuous and show highly-variable strikes. These factors are governed by the shape of minibasins and the angle of collisions between minibasins.

11 References

ADAM, J., URAI, J., WIENEKE, B., ONCKEN, O., PFEIFFER, K., KUKOWSKI, N., LOHRMANN, J., HOTH, S., VAN DER ZEE, W. & SCHMATZ, J. (2005) Shear Localisation and Strain Distribution During Tectonic Faulting—New Insights from Granular-Flow Experiments and High-Resolution Optical Image Correlation Techniques. *Journal of Structural Geology*, **27,** 283-301.

BABY, P., CALDERÓN, Y., BRUSSET, S., RODDAZ, M., BRICHAU, S., EUDE, A., CALVES, G., CALDERÓN, Y., QUISPE, A. & RAMIREZ, L. (2018) The Peruvian Sub-Andean Foreland Basin System: Structural Overview, Geochronologic Constraints, and Unexplored Plays. *AAPG Memoirs, Petroleum basins and hydrocarbon potential of the Andes of Peru and Bolivia*, **117**, 91-120.

BUTLER, R.W. (2019) Syn-Kinematic Strata Influence the Structural Evolution of Emergent Fold–Thrust Belts. *Geological Society, London, Special Publications*, **490,** SP490-2019-2014.

CALLOT, J.P., JAHANI, S. & LETOUZEY, J. (2007) The Role of Pre-Existing Diapirs in Fold and Thrust Belt Development. In: *Thrust Belts and Foreland Basins*, 309-325. Springer.

CALLOT, J.P., TROCME, V., LETOUZEY, J., ALBOUY, E., JAHANI, S. & SHERKATI, S. (2012) Pre-Existing Salt Structures and the Folding of the Zagros Mountains. *Salt Tectonics, Sediments and Prospectivity*, **363,** 545-561.

CALLOT, J.P., RIBES, C., KERGARAVAT, C., BONNEL, C., TEMIZ, H., POISSON, A., VRIELYNCK, B., SALEL, J.F. & RINGENBACH, J.C. (2014) Salt Tectonics in the Sivas Basin (Turkey): Crossing Salt Walls and Minibasins. *Bulletin De La Societe Geologique De France*, **185,** 33-42.

CALLOT, J.P., SALEL, J.F., LETOUZEY, J., DANIEL, J.M. & RINGENBACH, J.C. (2016) Three-Dimensional Evolution of Salt-Controlled Minibasins: Interactions, Folding, and Megaflap Development. *AAPG Bulletin*, **100,** 1419-1442.

COSTA, E. & VENDEVILLE, B.C. (2002) Experimental Insights on the Geometry and Kinematics of Fold-and-Thrust Belts above Weak, Viscous Evaporitic Decollement. *Journal of Structural Geology*, **24,** 1729-1739.

COTTON, J.T. & KOYI, H.A. (2000) Modeling of Thrust Fronts above Ductile and Frictional Detachments: Application to Structures in the Salt Range and Potwar Plateau, Pakistan. *Geological Society of America Bulletin*, **112,** 351-363.

DARNAULT, R., CALLOT, J.P., BALLARD, J.F., FRAISSE, G., MENGUS, J.M. & RINGENBACH, J.C. (2016) Control of Syntectonic Erosion and Sedimentation on Kinematic Evolution of a Multidecollement Fold and Thrust Zone: Analogue Modeling of Folding in the Southern Subandean of Bolivia. *Journal of Structural Geology*, **89,** 30-43.

DAVIS, D.M. & ENGELDER, T. (1985) The Role of Salt in Fold-and-Thrust Belts. *Tectonophysics*, **119,** 67-88.

DIEGEL, F.A., KARLO, J., SCHUSTER, D., SHOUP, R. & TAUVERS, P. (1995) Cenozoic Structural Evolution and Tectono-Stratigraphic Framework of the Northern Gulf Coast Continental Margin. *AAPG Memoirs, Salt Tectonics: A Global Perspective*, **65**, 109-151.

Dooley, T.P., Jackson, M.P.A. & Hudec, M.R. (2007) Initiation and Growth of Salt-Based Thrust Belts on Passive Margins: Results from Physical Models. *Basin Research*, **19,** 165-177.

Dooley, T.P., Jackson, M.P.A. & Hudec, M.R. (2009) Inflation and Deflation of Deeply Buried Salt Stocks During Lateral Shortening. *Journal of Structural Geology*, **31,** 582-600.

Dooley, T.P., Jackson, M.P. & Hudec, M.R. (2013) Coeval Extension and Shortening above and Below Salt Canopies on an Uplifted, Continental Margin: Application to the Northern Gulf of Mexico. *AAPG Bulletin*, **97,** 1737-1764.

Dooley, T.P., Jackson, M.P.A. & Hudec, M.R. (2015) Breakout of Squeezed Stocks: Dispersal of Roof Fragments, Source of Extrusive Salt and Interaction with Regional Thrust Faults. *Basin Research*, **27,** 3-25.

Dooley, T.P. (2020) Physical Models - Shortening of Isolated-Minibasin Provinces. *Figshare*. https://doi.org/10.6084/m9.figshare.12659828.v1

Duffy, O.B., Fernandez, N., Hudec, M.R., Jackson, M.P.A., Burg, G., Dooley, T.P. & Jackson, C.A.L. (2017) Lateral Mobility of Minibasins During Shortening: Insights from the SE Precaspian Basin, Kazakhstan. *Journal of Structural Geology*, **97,** 257-276.

Duffy, O.B., Dooley, T.P., Hudec, M.R., Jackson, M.P.A., Fernandez, N., Jackson, C.A.L. & Soto, J.I. (2018) Structural Evolution of Salt-Influenced Fold-and-Thrust Belts: A Synthesis and New Insights from Basins Containing Isolated Salt Diapirs. *Journal of Structural Geology*, **114,** 206-221.

Duffy, O.B., Fernandez, N., Peel, F.J., Hudec, M.R., Dooley, T.P. & Jackson, C.A.L. (2020) Obstructed Minibasins on a Salt-Detached Slope: An Example from above the Sigsbee Canopy, Northern Gulf of Mexico. *Basin Research*. **32 (3),** 505-524.

Fernandez, N., Duffy, O.B., Hudec, M.R., Jackson, M.P.A., Burg, G., Jackson, C.A.L. & Dooley, T.P. (2017) The Origin of Salt-Encased Sediment Packages: Observations from the SE Precaspian Basin (Kazakhstan). *Journal of Structural Geology*, **97,** 237-256.

Fernandez, N., Duffy, O.B., Peel, F. & Hudec, M.R. (2020a) Influence of Minibasin Obstruction on Canopy Dynamics in the Northern Gulf of Mexico. *Basin Research*. https://doi.org/10.1111/bre.12480

Fernandez, N., Duffy, O.B., Jackson, C.A.-L., Dooley, T., Hudec, M.R. & Kaus, J.P. (2020b) How Fast Can Minibasins Translate Down a Slope? Observations from 2d Numerical Models. *EarthArXiv Pre-print.* https://doi.org/10.31223/X55S31

Fernandez, N., Hudec, M.R., Jackson, C.A.-L., Dooley, T.P. & Duffy, O.B. (2020c) The Competition for Salt and Kinematic Interactions between Minibasins During Density-Driven Subsidence: Observations from Numerical Models. *Petroleum Geoscience*, **26,** 3-15.

Fiduk, J.C., Robertson, V., Clippard, M., Jamieson, G.A. & Power, S. (2016) Extensional Salt Keels Detached on Eocene-Oligocene Sediments in the Deepwater Northern Gulf of Mexico: Insights into Canopy Advancement, Salt-Sediment Interplay, and Evidence for Unrecognized Mass Sediment Displacement. *GCAGS Journal*, 5, 47–63.

Flinch, J.F. & Soto, J.I. (2017) Allochthonous Triassic and Salt Tectonic Processes in the Betic-Rif Orogenic Arc. In: *Permo-Triassic Salt Provinces of Europe, North Africa and the Atlantic Margins*, 417-446. Elsevier.

Fort, X., Brun, J.P. & Chauvel, F. (2004) Salt Tectonics on the Angolan Margin, Synsedimentary Deformation Processes. *AAPG Bulletin*, **88,** 1523-1544.

Frey, M.G. (1973) Influence of Salina Salt on Structure in New-York-Pennsylvania Part of Appalachian-Plateau. *AAPG Bulletin*, **57,** 1027-1037.

Ge, H., Jackson, M.P. & Vendeville, B.C. (1997) Kinematics and Dynamics of Salt Tectonics Driven by Progradation. *AAPG Bulletin,* **81,** 398-423.

Ge, Z.Y., Gawthorpe, R.L., Rotevatn, A., Zijerveld, L., Jackson, C.A.L. & Oluboyo, A. (2019) Minibasin Depocentre Migration During Diachronous Salt Welding, Offshore Angola. *Basin Research*.

Ghanadian, M., Faghih, A., Fard, I.A., Kusky, T. & Maleki, M. (2017) On the Role of Incompetent Strata in the Structural Evolution of the Zagros Fold-Thrust Belt, Dezful Embayment, Iran. *Marine and Petroleum Geology*, **81,** 320-333.

Granado, P., Roca, E., Strauss, P., Pelz, K. & Muñoz, J.A. (2018) Structural Styles in Fold-and-Thrust Belts Involving Early Salt Structures: The Northern Calcareous Alps (Austria). *Geology*, **47 (1),** 51-54.

Grelaud, S., Sassi, W., de Lamotte, D.F., Jaswal, T. & Roure, F. (2002) Kinematics of Eastern Salt Range and South Potwar Basin (Pakistan): A New Scenario. *Marine and Petroleum Geology*, **19,** 1127-1139.

Guellec, S., Lajat, D., Mascle, A., Roure, F. & Tardy, M. (1990) Deep Seismic Profiling and Petroleum Potential in the Western Alps - Constraints with Ecors Data, Balanced Cross-Sections and Hydrocarbon Modeling. *Potential of Deep Seismic Profiling for Hydrocarbon Exploration*, **48,** 425-437.

Guezou, J.-C., Temiz, H., Poisson, A. & Gürsoy, H. (1996) Tectonics of the Sivas Basin: The Neogene Record of the Anatolian Accretion Along the Inner Tauric Suture. *International Geology Review*, **38,** 901-925.

Harrison, J.C. & Jackson, M.P.A. (2014) Exposed Evaporite Diapirs and Minibasins above a Canopy in Central Sverdrup Basin, Axel Heiberg Island, Arctic Canada. *Basin Research*, **26,** 567-596.

Hassanpour, J., Jahani, S., Ghassemi, M.R., Alavi, S.A. & Zeinali, F. (2018) Evolution of the Karebas Fault System and Adjacent Folds, Central Zagros Fold-and-Thrust Belt, Iran: Role of Pre-Existing Halokinesis (Salt Structures and Minibasins) and Detachment Levels. *Journal of Asian Earth Sciences*, **164,** 125-142.

Hassanpour, J., Yassaghi, A., Muñoz, J.A. & Jahani, S. (2020) Salt Tectonics in a Double Salt-Source Layer Setting (Eastern Persian Gulf, Iran): Insights from Interpretation of Seismic Profiles and Sequential Cross-Section Restoration. *Basin Research*. https://doi.org/10.1111/bre.12459

Hermoza, W., Brusset, S., Baby, P., Gil, W., Roddaz, M., Guerrero, N. & Bolaños, R. (2005) The Huallaga Foreland Basin Evolution: Thrust Propagation in a Deltaic Environment, Northern Peruvian Andes. *Journal of South American Earth Sciences*, **19,** 21-34.

Hudec, M.R. & Jackson, M.P. (2007) Terra Infirma: Understanding Salt Tectonics. *Earth-Science Reviews*, **82,** 1-28.

Hudec, M.R., Jackson, M.P. & Schultz-Ela, D.D. (2009) The Paradox of Minibasin Subsidence into Salt: Clues to the Evolution of Crustal Basins. *Geological Society of America Bulletin*, **121,** 201-221.

Iribarne, M., Callot, P., Quevedo, C.D., Márquez, S., Castillo, E., Chung, J., Seminario, F., Ghiglione, M.C., Sempere, T. & Kelly, R. (2018) Stratigraphy, Structural Styles, and Hydrocarbon Potential of the Ene Basin: An Exploration Opportunity in the Sub-Andean Fold-and-Thrust Belt of Peru. *AAPG Memoirs, Petroleum basins and hydrocarbon potential of the Andes of Peru and Bolivia*, **117**, 297-322.

Jackson, M. & Harrison, J. (2006) An Allochthonous Salt Canopy on Axel Heiberg Island, Sverdrup Basin, Arctic Canada. *Geology*, **34,** 1045-1048.

Jackson, M.P. & Hudec, M.R. (2017) *Salt Tectonics: Principles and Practice*. Cambridge University Press.

Jackson, C.A.L., Duffy, O.B., Fernandez, N., Dooley, T.P., Hudec, M.R., Jackson, M.P. & Burg, G. (2020) The Stratigraphic Record of Minibasin Subsidence, Precaspian Basin, Kazakhstan. *Basin Research*. **32 (4),** 739-763.

Jahani, S., Callot, J.P., Letouzey, J. & Frizon de Lamotte, D. (2009) The Eastern Termination of the Zagros Fold-and-Thrust Belt, Iran: Structures, Evolution, and Relationships between Salt Plugs, Folding, and Faulting. *Tectonics*, **28**. TC6004.

Jahani, S., Hassanpour, J., Mohammadi-Firouz, S., Letouzey, J., de Lamotte, D.F., Alavi, S.A. & Soleimany, B. (2017) Salt Tectonics and Tear Faulting in the Central Part of the Zagros Fold-Thrust Belt, Iran. *Marine and Petroleum Geology*, **86,** 426-446.

Kergaravat, C., Ribes, C., Legeay, E., Callot, J.P., Kavak, K.S. & Ringenbach, J.C. (2016) Minibasins and Salt Canopy in Foreland Fold-and-Thrust Belts: The Central Sivas Basin, Turkey. *Tectonics*, **35,** 1342-1366.

Kergaravat, C., Ribes, C., Callot, J.P. & Ringenbach, J.C. (2017) Tectono-Stratigraphic Evolution of Salt-Controlled Minibasins in a Fold and Thrust Belt, the Oligo-Miocene Central Sivas Basin. *Journal of Structural Geology*, **102,** 75-97.

Krantz, R.W. (1991) Measurements of Friction Coefficients and Cohesion for Faulting and Fault Reactivation in Laboratory Models Using Sand and Sand Mixtures. *Tectonophysics*, **188,** 203-207.

Kurtman, F. (1973) Sivas-Hafik-Zara Ve Imranli Bölgesinin Jeolojik Ve Tektonik Yapisi. *Bull. General Directorate of Mineral Research and Exploration of Turkey*, **80,** 1-32.

Lacombe, O. & Bellahsen, N. (2016) Thick-Skinned Tectonics and Basement-Involved Fold-Thrust Belts: Insights from Selected Cenozoic Orogens. *Geological Magazine*, **153,** 763-810.

Laubscher, H.P. (1961) Die Fernschubhypothese Der Jurafaltung. *Eclogae Geologicae Helvetiae*, **54,** 222-282.

Legeay, E., Ringenbach, J.-C., Kergaravat, C., Pichat, A., Mohn, G., Vergés, J., Kavak, K.S. & Callot, J.-P. (2019) Structure and Kinematics of the Central Sivas Basin (Turkey): Salt Deposition and Tectonics in an Evolving Fold-and-Thrust Belt. *Geological Society, London, Special Publications*, **490,** SP490-2019-2092.

Leitner, C. & Spötl, C. (2017) The Eastern Alps: Multistage Development of Extremely Deformed Evaporites. In: *Permo-Triassic Salt Provinces of Europe, North Africa and the Atlantic Margins*, 467-482. Elsevier.

Letouzey, J., Colletta, B., Vially, R. & Chermette, J.C. (1995) Evolution of Salt-Related Structures in Compressional Settings. *Salt Tectonics: A Global Perspective*, **65,** 41-60.

Lopez-Mir, B., Munoz, J.A. & Senz, J.G. (2014) Restoration of Basins Driven by Extension and Salt Tectonics: Example from the Cotiella Basin in the Central Pyrenees. *Journal of Structural Geology*, **69,** 147-162.

McClay, K. (1990) Deformation Mechanics in Analogue Models of Extensional Fault Systems. *Geological Society, London, Special Publications*, **54,** 445-453.

McClay, K., Tamara, J., Hammerstein, J., Mora, A., Zamora, G. & Uzkeda, H. (2018) Sub-Andean Thick and Thin-Skinned Thrust Systems of Southeastern Peru and Bolivia—a Review. *AAPG Memoirs, Petroleum basins and hydrocarbon potential of the Andes of Peru and Bolivia*, **117**, 35-62.

Morley, C.K., King, R., Hillis, R., Tingay, M. & Backe, G. (2011) Deepwater Fold and Thrust Belt Classification, Tectonics, Structure and Hydrocarbon Prospectivity: A Review. *Earth-Science Reviews*, **104,** 41-91.

Najafi, M., Yassaghi, A., Bahroudi, A., Vergés, J. & Sherkati, S. (2014) Impact of the Late Triassic Dashtak Intermediate Detachment Horizon on Anticline Geometry in the Central Frontal Fars, Se Zagros Fold Belt, Iran. *Marine and Petroleum Geology*, **54,** 23-36.

Nilsen, K.T., Vendeville, B.C. & Johansen, J.T. (1995) Influence of Regional Tectonics on Halokinesis in the Nordkapp Basin, Barents Sea. *Salt Tectonics: A Global Perspective*, **65,** 413-436.

Peel, F.J., Travis, C.J. & Hossack, J.R. (1995) Genetic Structural Provinces and Salt Tectonics of the Cenozoic Offshore Us Gulf of Mexico: A Preliminary Analysis. *Salt Tectonics: A Global Perspective*, **65,** 153-175.

Pilcher, R.S., Kilsdonk, B. & Trude, J. (2011) Primary Basins and Their Boundaries in the Deep-Water Northern Gulf of Mexico: Origin, Trap Types, and Petroleum System Implications. *AAPG Bulletin*, **95,** 219-240.

Poisson, A., Guezou, J., Ozturk, A., Inan, S., Temiz, H., Gürsöy, H., Kavak, K.S. & Özden, S. (1996) Tectonic Setting and Evolution of the Sivas Basin, Central Anatolia, Turkey. *International Geology Review*, **38,** 838-853.

Reber, J.E., Cooke, M.L. & Dooley, T.P. (2020) What Model Material to Use? A Review on Rock Analogs for Structural Geology and Tectonics. *Earth-Science Reviews*, **202,** 103107.

Ribes, C., Kergaravat, C., Bonnel, C., Crumeyrolle, P., Callot, J.P., Poisson, A., Temiz, H. & Ringenbach, J.C. (2015) Fluvial Sedimentation in a Salt-Controlled Mini-Basin: Stratal Patterns and Facies Assemblages, Sivas Basin, Turkey. *Sedimentology*, **62,** 1513-1545.

Ribes, C., Kergaravat, C., Crumeyrolle, P., Lopez, M., Bonnel, C., Poisson, A., Kavak, K.S., Callot, J.P. & Ringenbach, J.C. (2017) Factors Controlling Stratal Pattern and Facies Distribution of Fluvio-Lacustrine Sedimentation in the Sivas Mini-Basins, Oligocene (Turkey). *Basin Research*, **29,** 596-621.

Ringenbach, J.-C., Salel, J.-F., Kergaravat, C., Ribes, C., Bonnel, C. & Callot, J.-P. (2013) Salt Tectonics in the Sivas Basin, Turkey: Outstanding Seismic Analogues from Outcrops. *First Break*, **31**. 93-101.

Rodriguez, W.G., Baby, P. & Ballard, J.-F. (2001) Structure Et Contrôle Paléogéographique De La Zone Subandine Péruvienne. *Comptes Rendus de l'Académie des Sciences-Series IIA-Earth and Planetary Science*, **333,** 741-748.

Rossi, D. & Storti, F. (2003) New Artificial Granular Materials for Analogue Laboratory Experiments: Aluminium and Siliceous Microspheres. *Journal of Structural Geology*, **25,** 1893-1899.

Rowan, M.G., Jackson, M.P. & Trudgill, B.D. (1999) Salt-Related Fault Families and Fault Welds in the Northern Gulf of Mexico. *AAPG Bulletin*, **83,** 1454-1484.

Rowan, M.G. & Vendeville, B.C. (2006) Foldbelts with Early Salt Withdrawal and Diapirism: Physical Model and Examples from the Northern Gulf of Mexico and the Flinders Ranges, Australia. *Marine and Petroleum Geology*, **23,** 871-891.

Ruh, J.B., Verges, J. & Burg, J.P. (2018) Shale-Related Minibasins Atop a Massive Olistostrome in an Active Accretionary Wedge Setting: Two-Dimensional Numerical Modeling Applied to the Iranian Makran. *Geology*, **46,** 791-794.

Schellart, W. (2000) Shear Test Results for Cohesion and Friction Coefficients for Different Granular Materials: Scaling Implications for Their Usage in Analogue Modelling. *Tectonophysics*, **324,** 1-16.

Sherkati, S. & Letouzey, J. (2004) Variation of Structural Style and Basin Evolution in the Central Zagros (Izeh Zone and Dezful Embayment), Iran. *Marine and Petroleum Geology*, **21,** 535-554.

Sherkati, S., Letouzey, J. & de Lamotte, D.F. (2006) Central Zagros Fold-Thrust Belt (Iran): New Insights from Seismic Data, Field Observation, and Sandbox Modeling. *Tectonics*, **25**. TC4007.

Snidero, M., Munoz, J.A., Carrera, N., Butille, M., Mencos, J., Motamedi, H., Piryaei, A. & Sabat, F. (2019) Temporal Evolution of the Darmadan Salt Diapir, Eastern Fars Region, Iran. *Tectonophysics*, **766,** 115-130.

Sommaruga, A., Mosar, J., Schori, M. & Gruber, M. (2017) The Role of the Triassic Evaporites Underneath the North Alpine Foreland. In: *Permo-Triassic Salt Provinces of Europe, North Africa and the Atlantic Margins*, 447-466. Elsevier.

Talbot, C.J. & Pohjola, V. (2009) Subaerial Salt Extrusions in Iran as Analogues of Ice Sheets, Streams and Glaciers. *Earth-Science Reviews*, **97,** 155-183.

Vergés, J., Goodarzi, M., Emami, H., Karpuz, R., Efstathiou, J. & Gillespie, P. (2011) Multiple Detachment Folding in Pusht-E Kuh Arc, Zagros: Role of Mechanical Stratigraphy. In: *Thrust fault-related folding: AAPG Memoir* **94**, 69–94.

Wagner III, B.H. & Jackson, M.P. (2011) Viscous Flow During Salt Welding. *Tectonophysics*, **510,** 309-326.

Weijermars, R. (1986) Flow Behaviour and Physical Chemistry of Bouncing Putties and Related Polymers in View of Tectonic Laboratory Applications. *Tectonophysics*, **124,** 325-358.

WEIJERMARS, R., JACKSON, M.T. & VENDEVILLE, B. (1993) Rheological and Tectonic Modeling of Salt Provinces. *Tectonophysics*, **217,** 143-174.

Figure 1

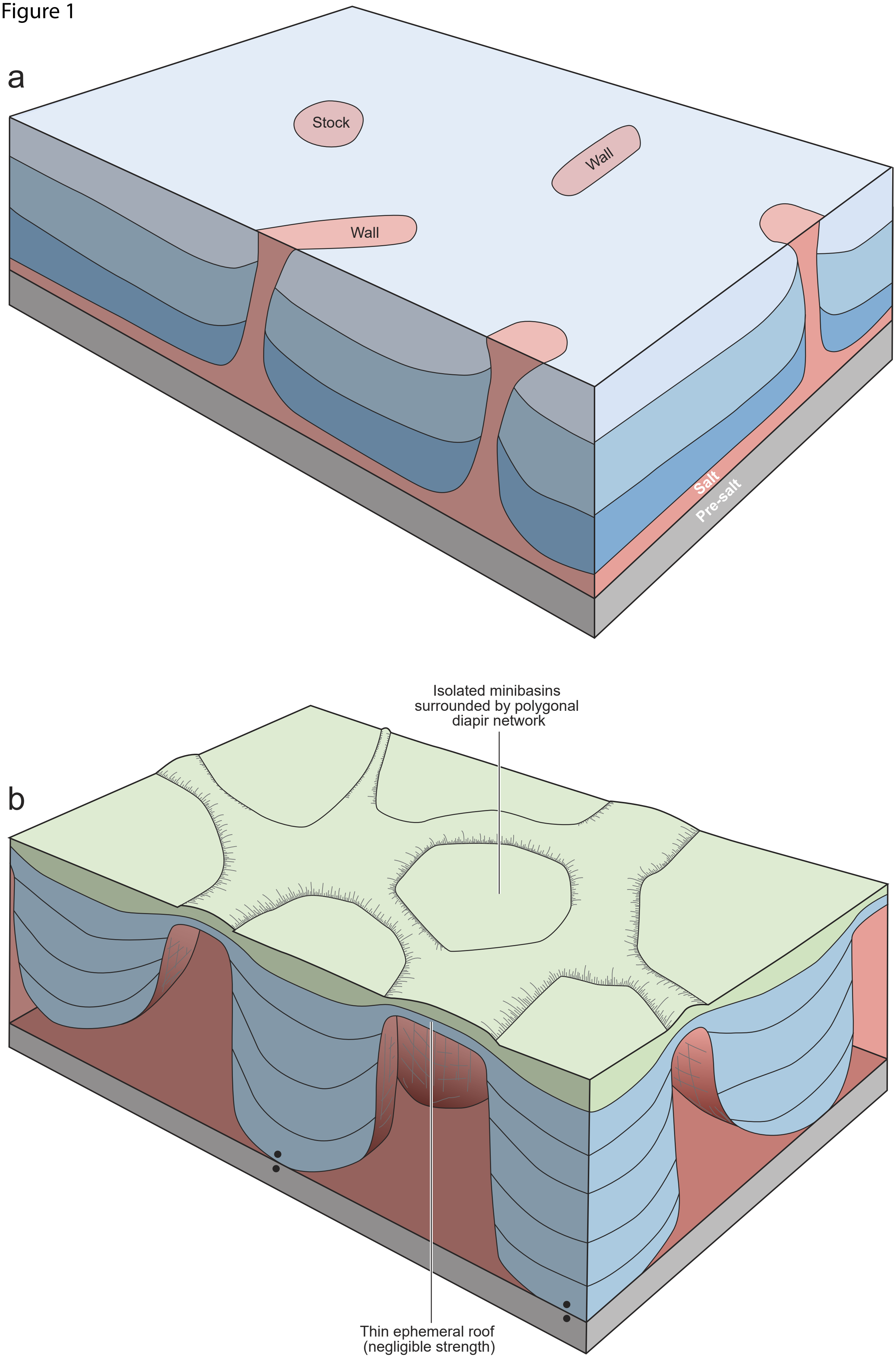
a
Stock
Wall
Wall
Salt
Pre-salt
b
Isolated minibasins
surrounded by polygonal
diapir network
Thin ephemeral roof
(negligible strength)

Figure 2

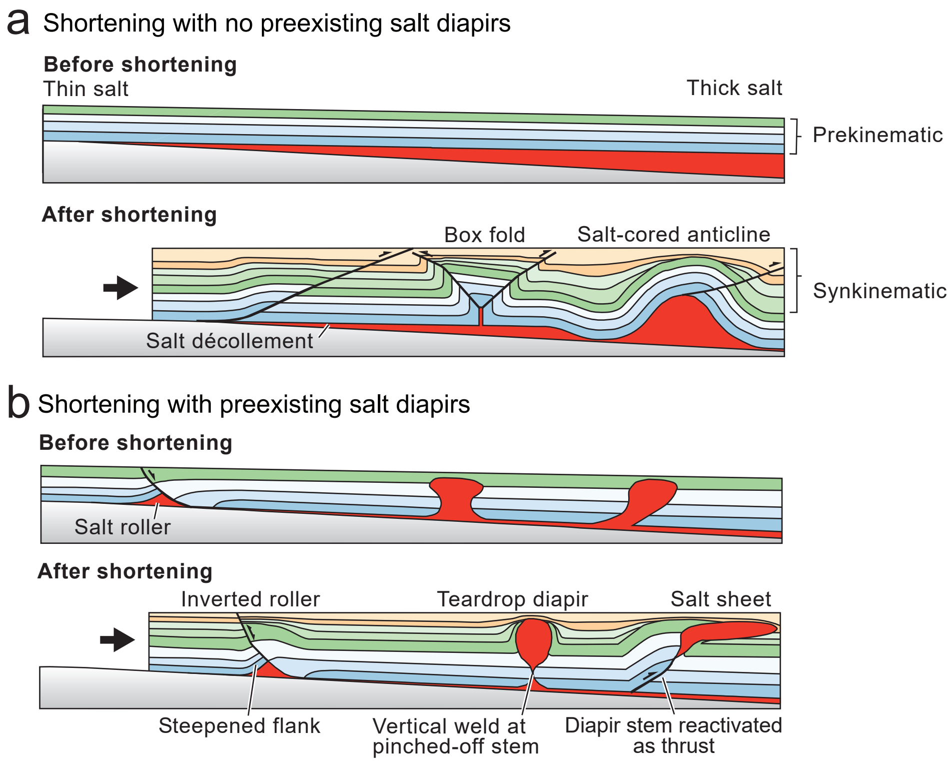
a Shortening with no preexisting salt diapirs
Before shortening
Thin salt
Thick salt
Prekinematic
After shortening
Box fold
Salt-cored anticline
Synkinematic
Salt décollement
b Shortening with preexisting salt diapirs
Before shortening
Salt roller
After shortening
Inverted roller
Teardrop diapir
Salt sheet
Steepened flank
Vertical weld at pinched-off stem
Diapir stem reactivated as thrust

Figure 3

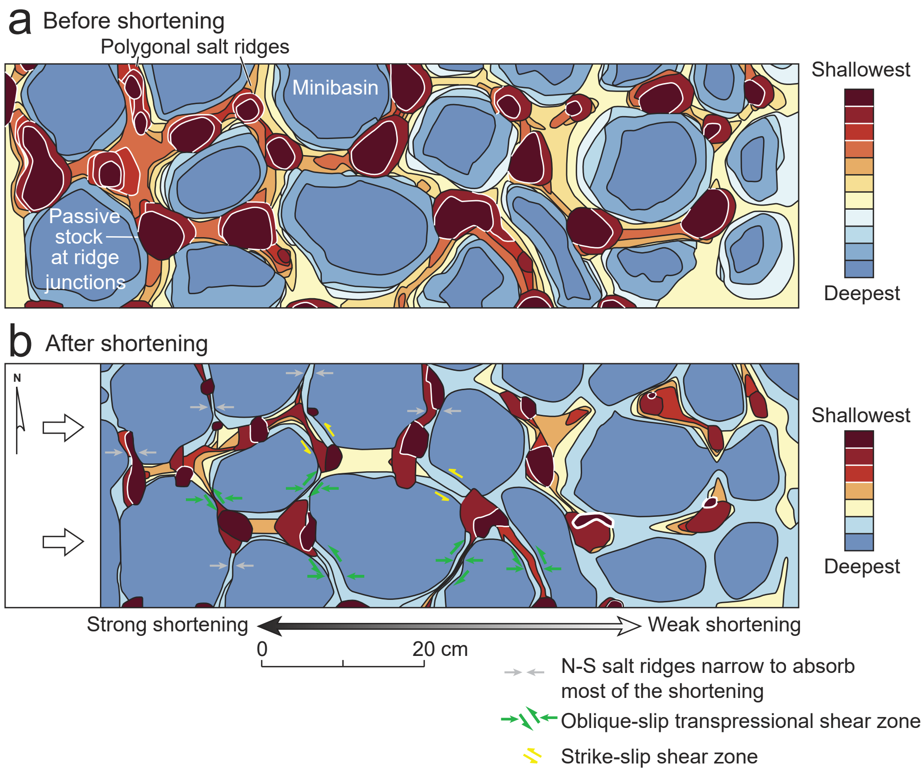

a Before shortening
Polygonal salt ridges
Minibasin
Passive stock at ridge junctions
Shallowest
Deepest
b After shortening
N
Shallowest
Deepest
Strong shortening
Weak shortening
0
20 cm
N-S salt ridges narrow to absorb most of the shortening
Oblique-slip transpressional shear zone
Strike-slip shear zone

Figure 4a and b

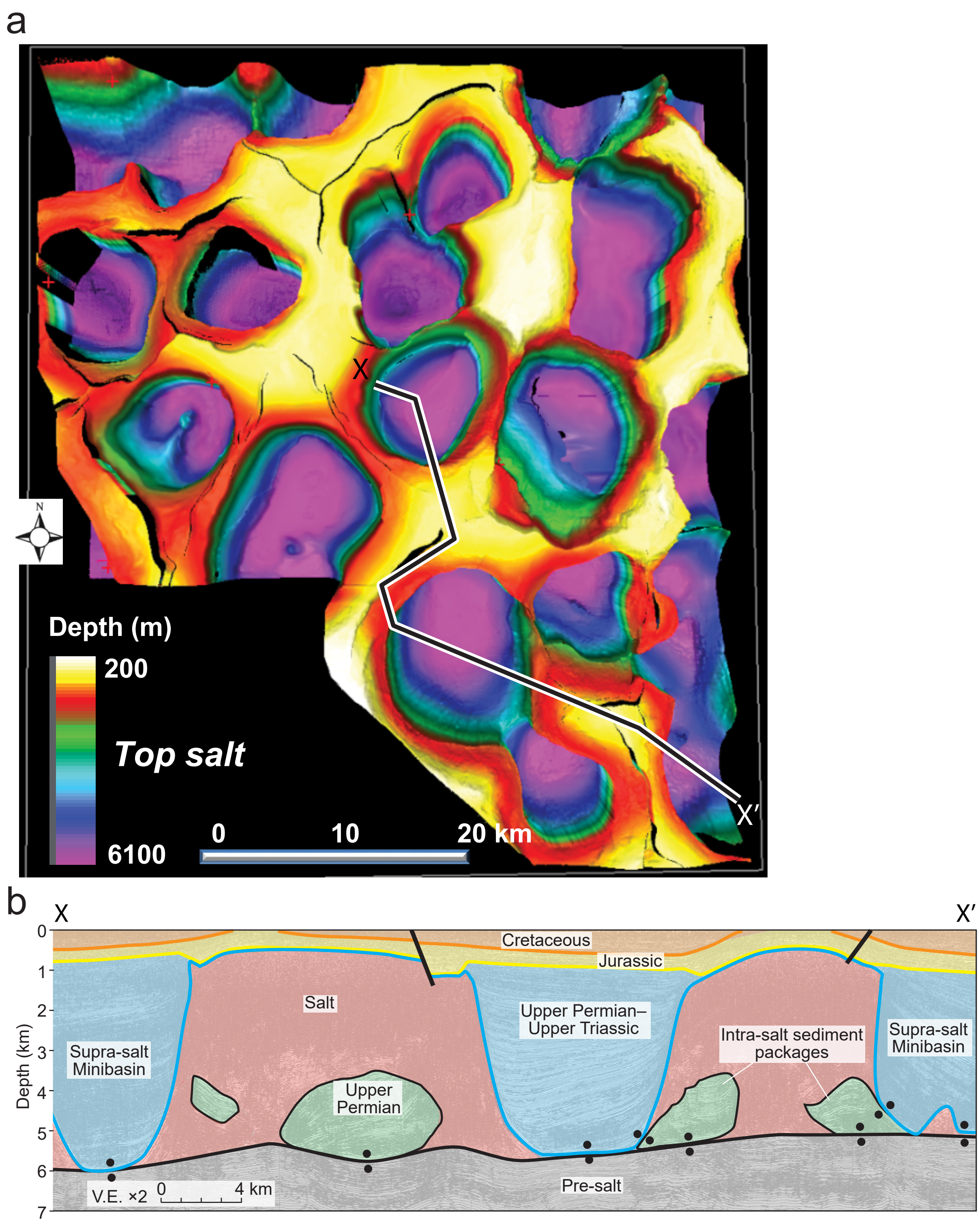

Figure 4c and d

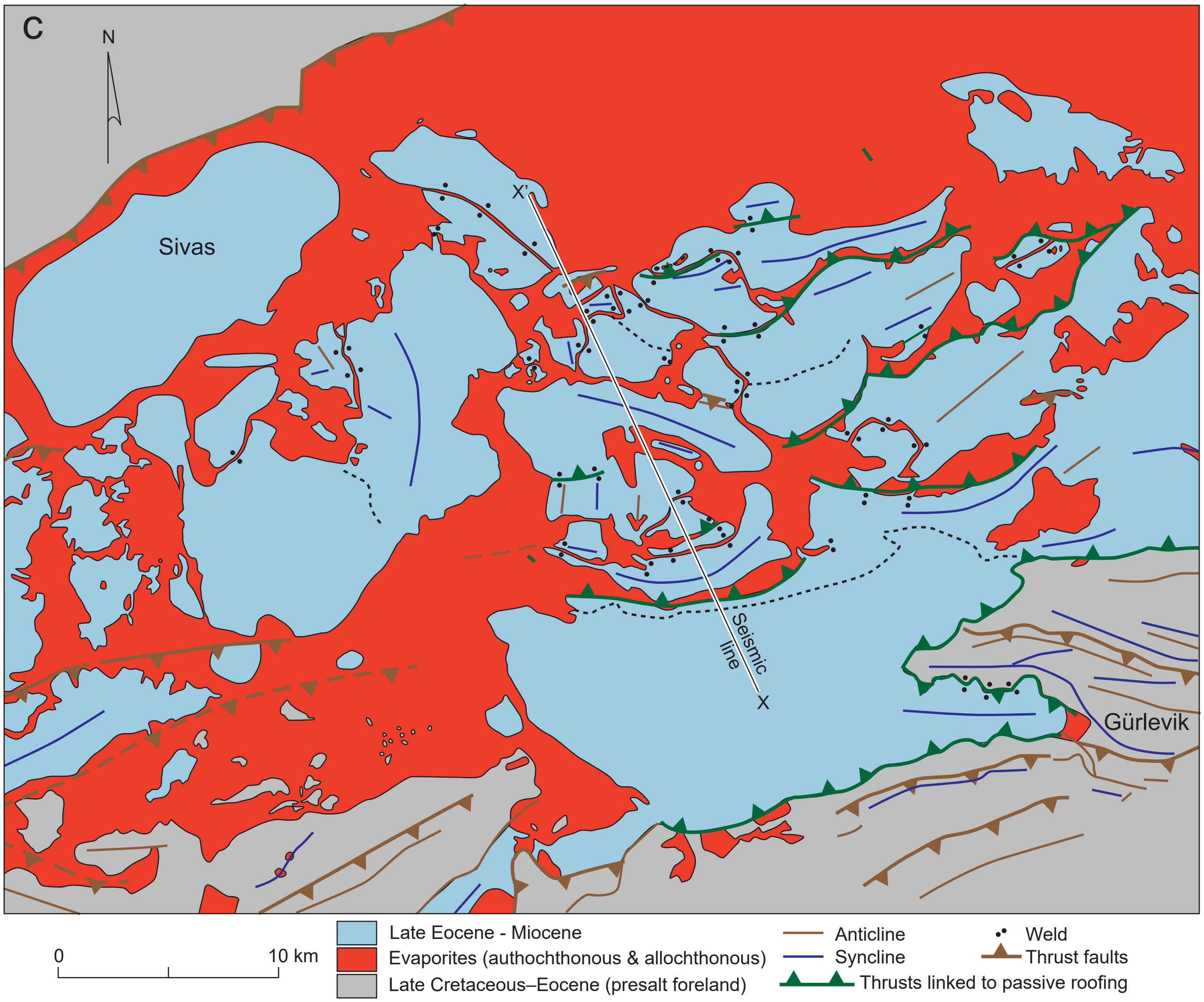

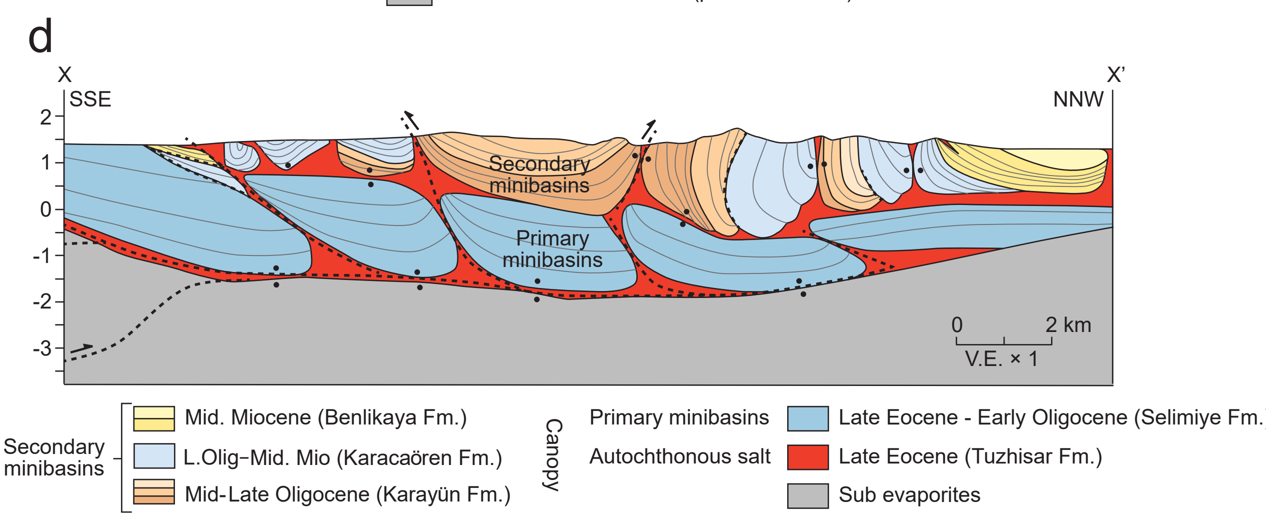

<table>
<tr><th>Model #</th><th>Regional dip</th><th>Source layer thickness</th><th>Total Shortening</th><th>Model design</th></tr>
<tr><td>Models 1a, 1b</td><td>0°</td><td>5 cm</td><td>33 cm</td><td rowspan="2">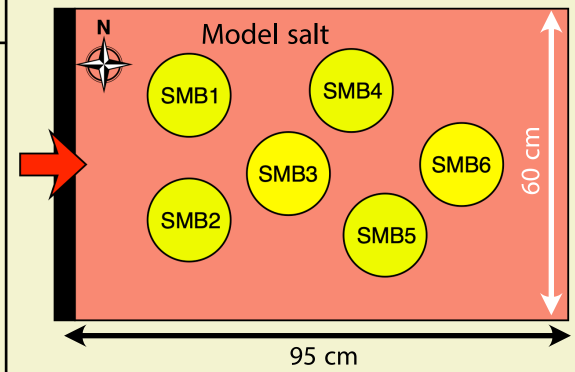
</td></tr>
<tr><td colspan="4">Model description:
6 supra salt minibasins (SMB), with diameters of 16 cm, sank into a 5-cm-thick salt basin. In Model 1a minibasins 3 and 6 subsided until about 1 cm from base of salt before the moving endwall began to shorten the basin. All other minibasins were 2 cm from base of salt before shortening. In Model 1b all minibasins were approximately 2 cm from base of salt before shortening was applied.

Sediments were continually added to the minibasins during shortening.</td></tr>
<tr><td>Model 2</td><td>0°</td><td>5 cm</td><td>12.5 cm</td><td rowspan="2">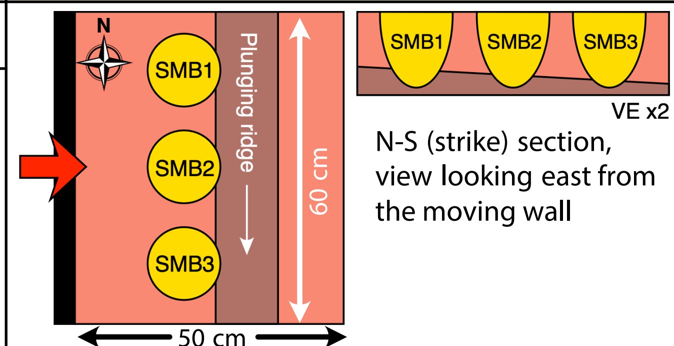
</td></tr>
<tr><td colspan="4">Model description:
3 supra salt minibasins (SMB), with 13 cm diameters, sank into a 5-cm-thick salt basin. A plunging base-salt high block, constructed from silica sands, was located to the right of the minibasins going from 2.5 cm to 0.5 cm across the model. Once the minibasins had subsided to just 0.5 cm from welding the salt basin was shortened.

Sediments were continually added to the minibasins during shortening.</td></tr>
<tr><td>Model 3</td><td>0°</td><td>5 cm</td><td>31</td><td rowspan="2">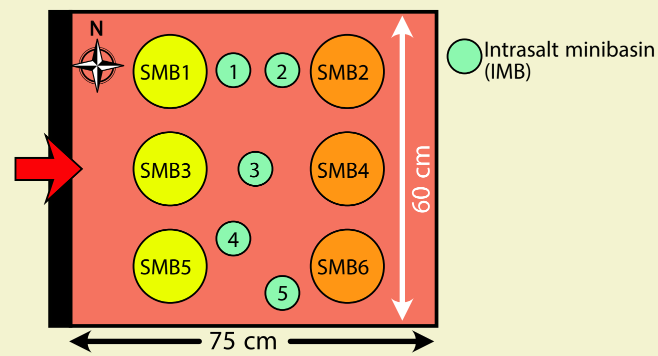
</td></tr>
<tr><td colspan="4">Model description:
5 small minibasins, with diameters of 7 cm, were sank into a 1.5-cm-thick model salt layer before being encased (IMB) in a further 3.5 cm of salt analog. 6 suprasalt minibasins (SMB), with diameters of 13 cm, were seeded into the salt basin on either side of the intrasalt minibasin (IMB) array. Suprasalt minibasins 4-6 were sunk to where they just welded, whereas suprasalt minibasins 1-3 subsided to 2.5 cm from base of salt before shortening began. Sediments were continually added to the SMBs during shortening.</td></tr>
</table>

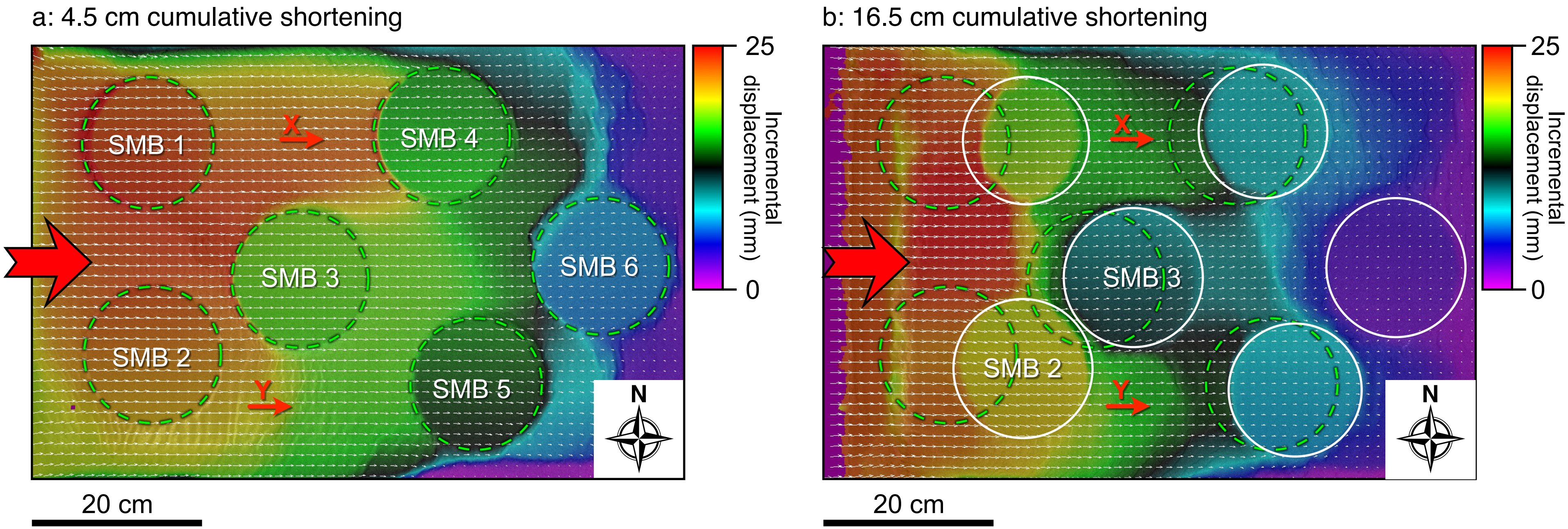

a: 4.5 cm cumulative shortening
b: 16.5 cm cumulative shortening
SMB 1
SMB 2
SMB 3
SMB 4
SMB 5
SMB 6
X
Y
N
25
0
Incremental displacement (mm)
20 cm

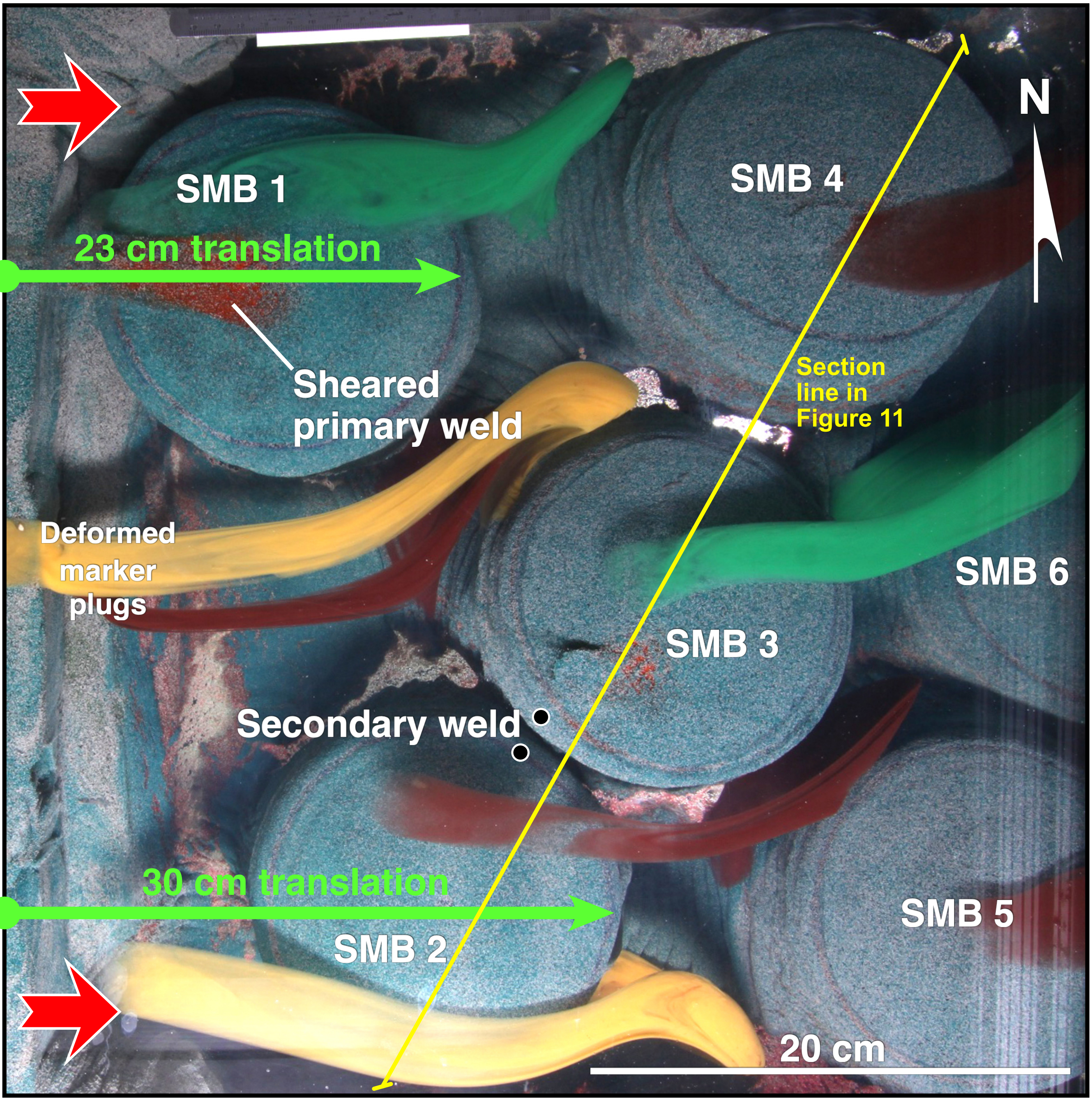
N
SMB 1
23 cm translation
SMB 4
Sheared
primary weld
Section
line in
Figure 11
Deformed
marker
plugs
SMB 6
SMB 3
Secondary weld
30 cm translation
SMB 2
SMB 5
20 cm

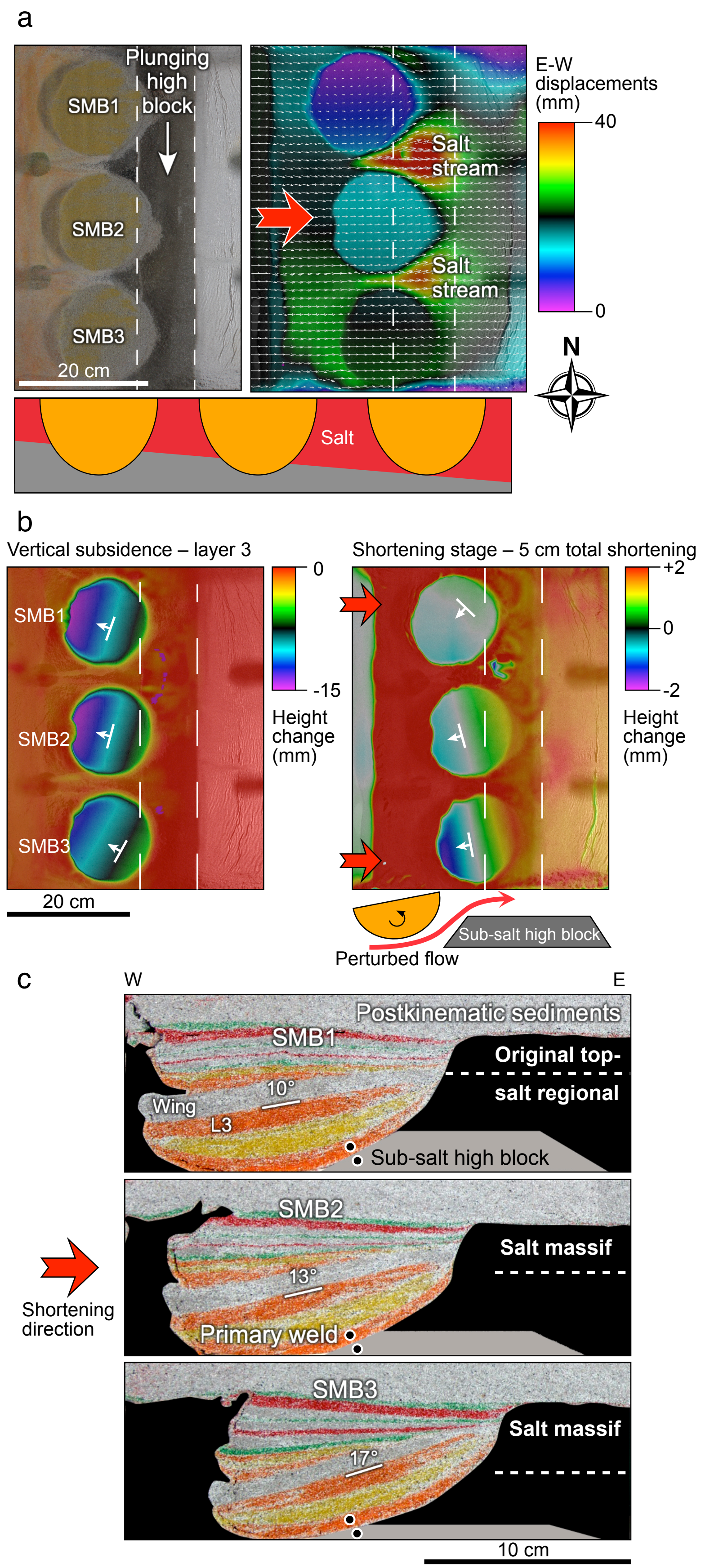
a
Plunging high block
SMB1
SMB2
SMB3
20 cm
Salt stream
Salt stream
E-W displacements (mm)
40
0
N
Salt
b
Vertical subsidence – layer 3
SMB1
SMB2
SMB3
0
-15
Height change (mm)
20 cm
Shortening stage – 5 cm total shortening
+2
0
-2
Height change (mm)
Sub-salt high block
Perturbed flow
c
W
E
Postkinematic sediments
SMB1
Original top-salt regional
10°
Wing
L3
Sub-salt high block
SMB2
Salt massif
13°
Primary weld
Shortening direction
SMB3
Salt massif
17°
10 cm

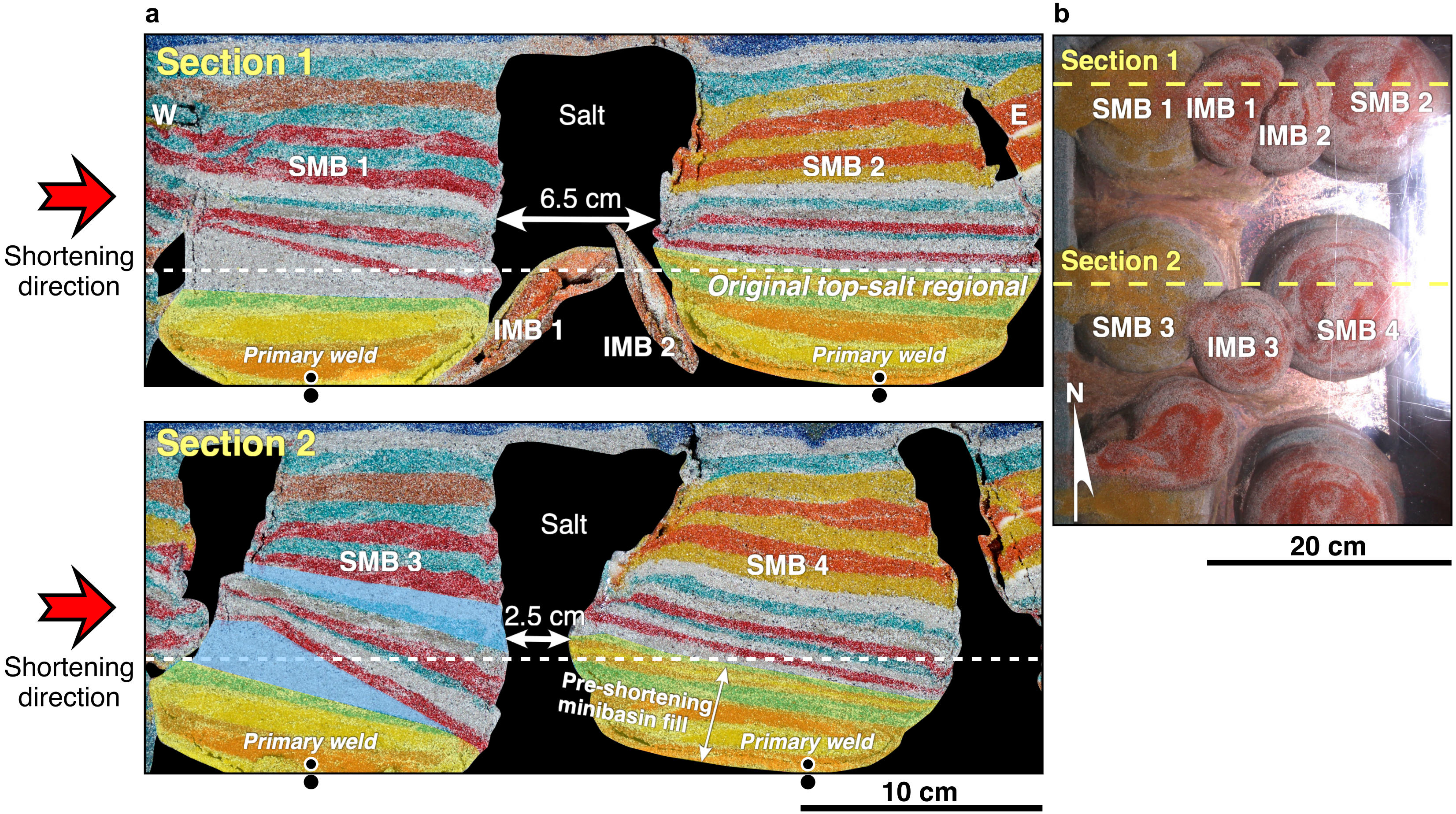

a
Section 1
W
E
Salt
SMB 1
SMB 2
6.5 cm
Original top-salt regional
IMB 1
IMB 2
Primary weld
Primary weld
Shortening direction
Section 2
Salt
SMB 3
SMB 4
2.5 cm
Pre-shortening minibasin fill
Primary weld
Primary weld
Shortening direction
10 cm
b
Section 1
SMB 1
IMB 1
IMB 2
SMB 2
Section 2
SMB 3
IMB 3
SMB 4
N
20 cm

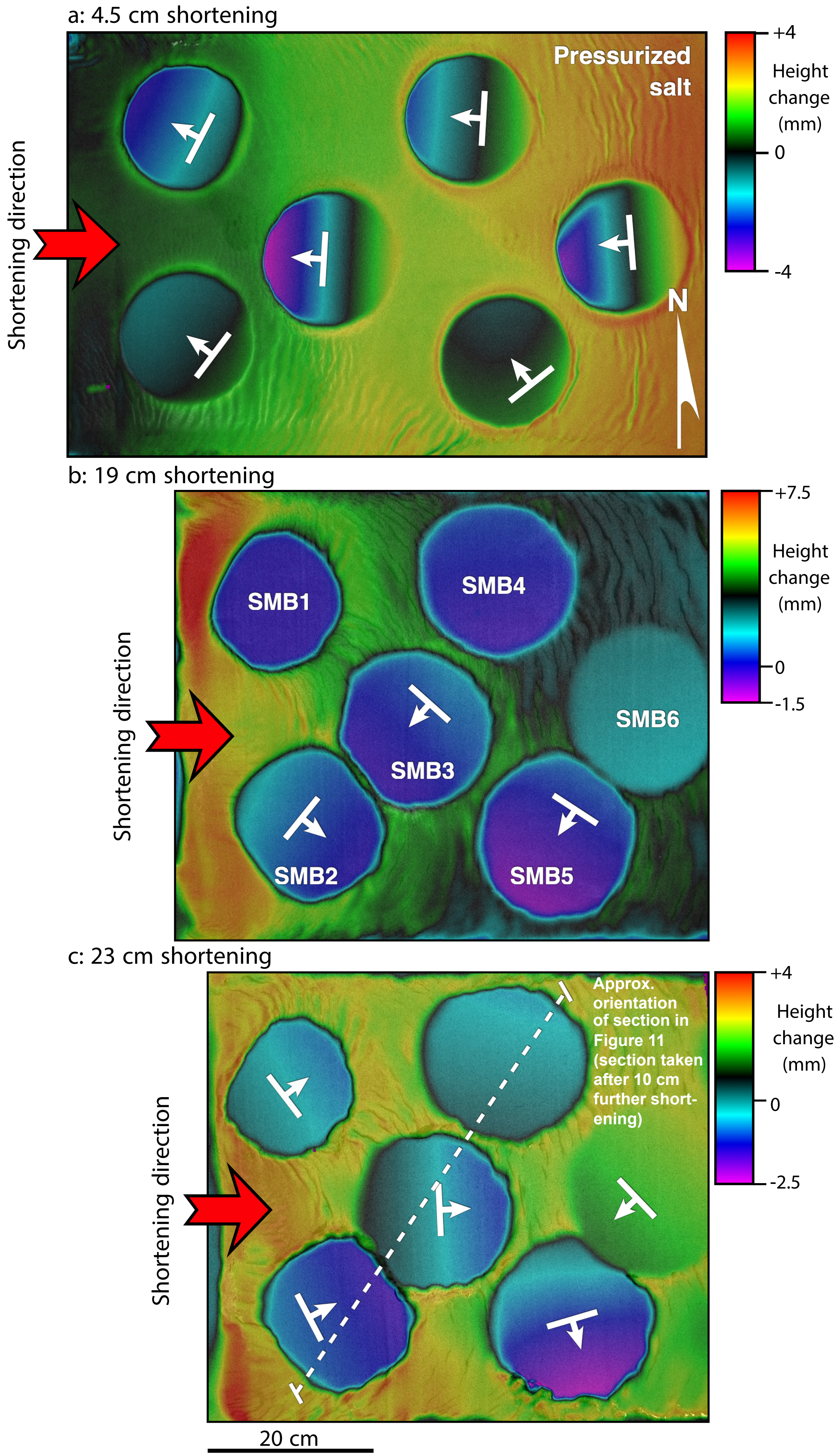

a: 4.5 cm shortening
Pressurized salt
Shortening direction
N
+4
Height change (mm)
0
-4
b: 19 cm shortening
SMB1
SMB2
SMB3
SMB4
SMB5
SMB6
Shortening direction
+7.5
Height change (mm)
0
-1.5
c: 23 cm shortening
Approx. orientation of section in Figure 11 (section taken after 10 cm further shortening)
Shortening direction
+4
Height change (mm)
0
-2.5
20 cm

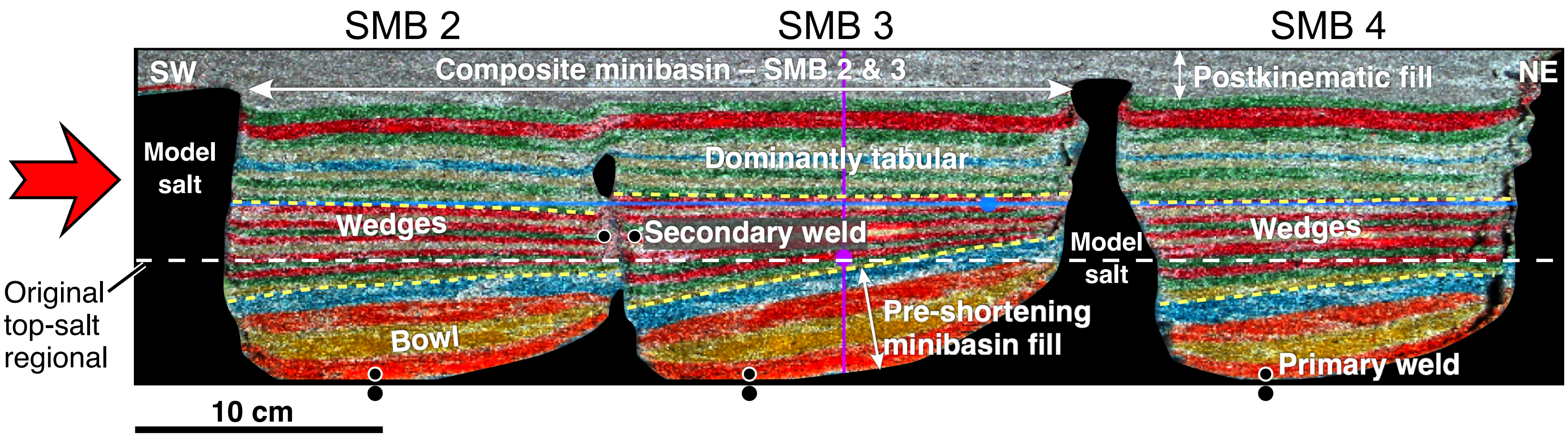

SMB 2
SMB 3
SMB 4
SW
Composite minibasin – SMB 2 & 3
Postkinematic fill
NE
Model salt
Dominantly tabular
Wedges
Secondary weld
Wedges
Model salt
Original top-salt regional
Pre-shortening minibasin fill
Bowl
Primary weld
10 cm

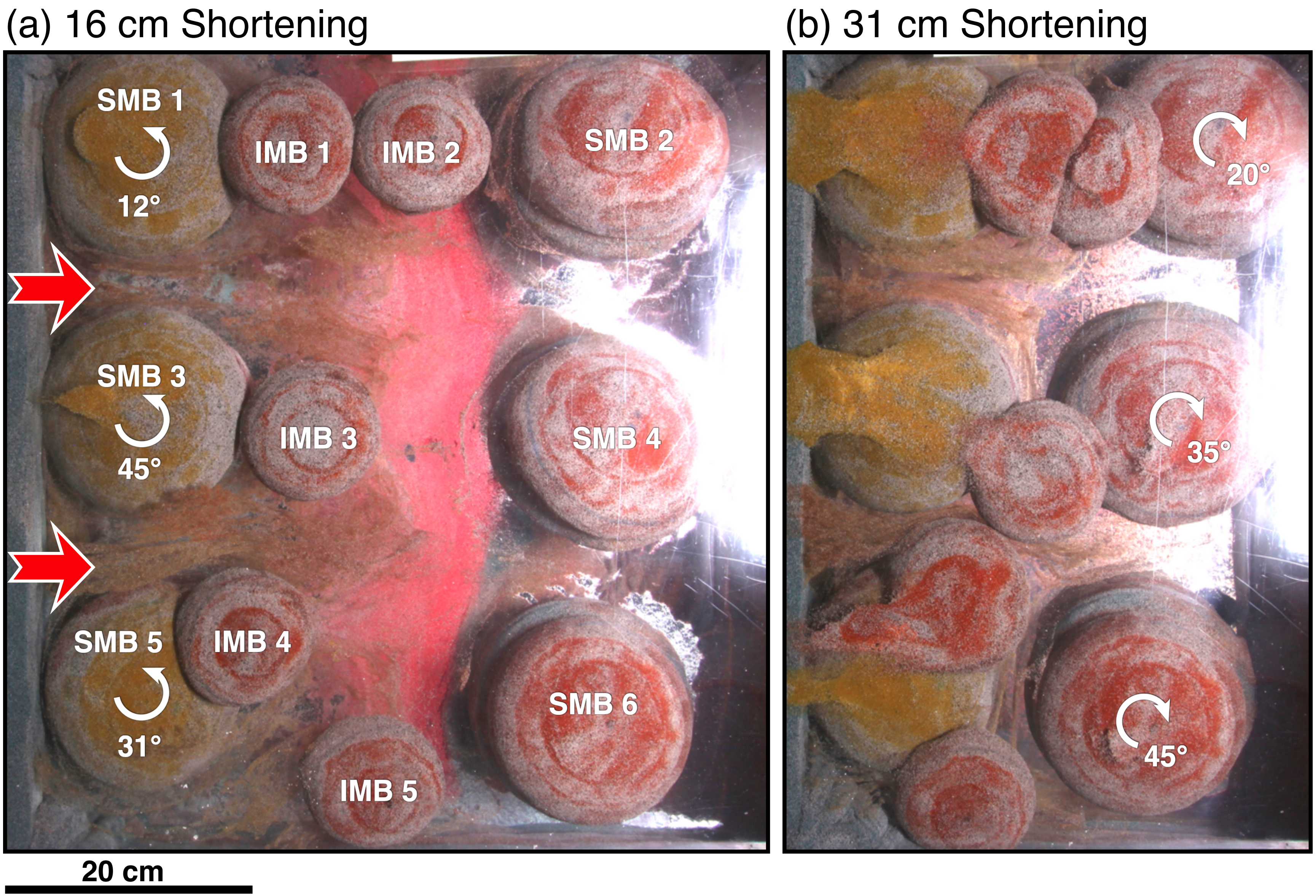
(a) 16 cm Shortening
(b) 31 cm Shortening
SMB 1
12°
IMB 1
IMB 2
SMB 2
SMB 3
45°
IMB 3
SMB 4
SMB 5
IMB 4
31°
SMB 6
IMB 5
20°
35°
45°
20 cm

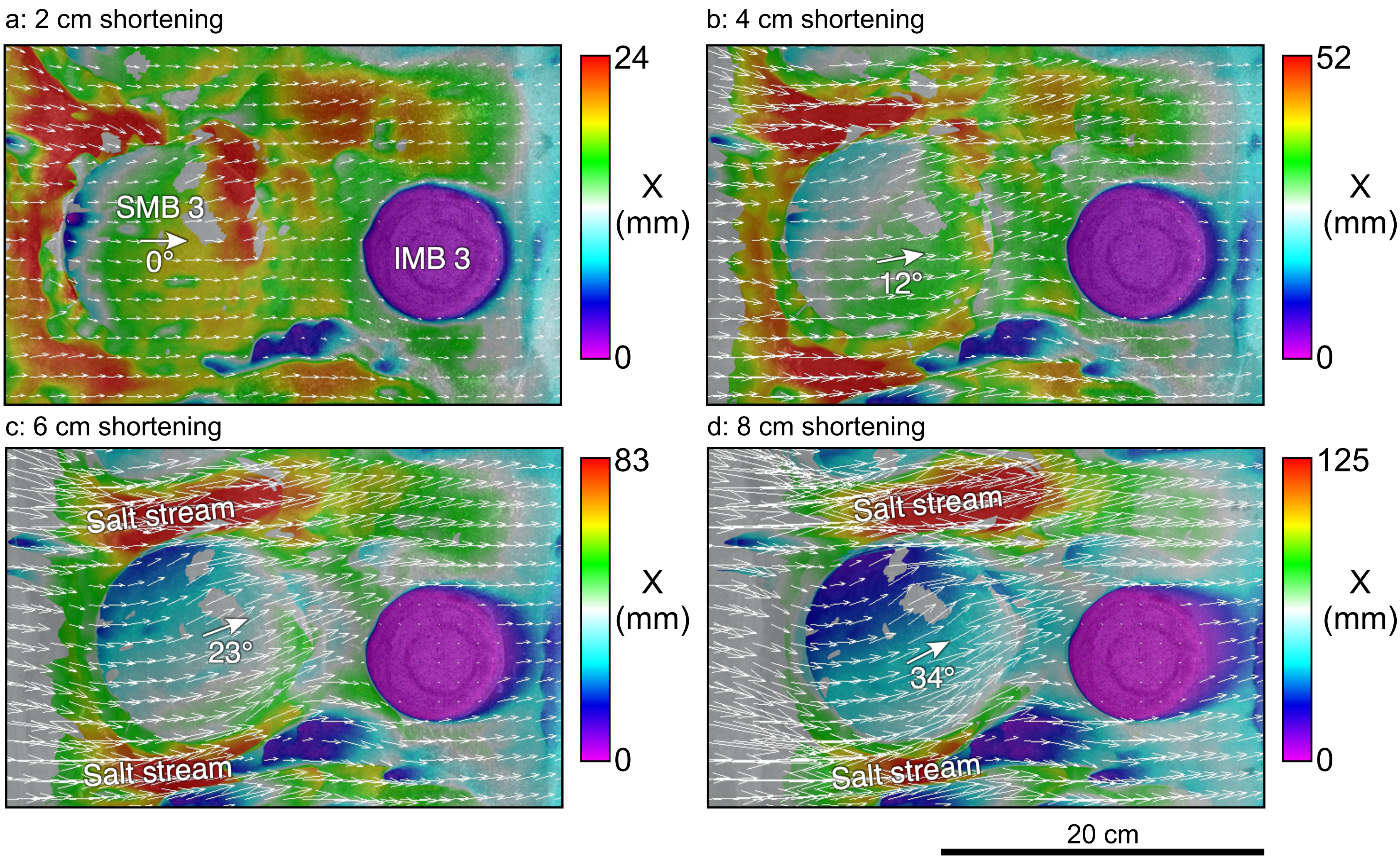
a: 2 cm shortening
SMB 3
0°
IMB 3
24
X (mm)
0
b: 4 cm shortening
12°
52
X (mm)
0
c: 6 cm shortening
Salt stream
23°
Salt stream
83
X (mm)
0
d: 8 cm shortening
Salt stream
34°
Salt stream
125
X (mm)
0
20 cm

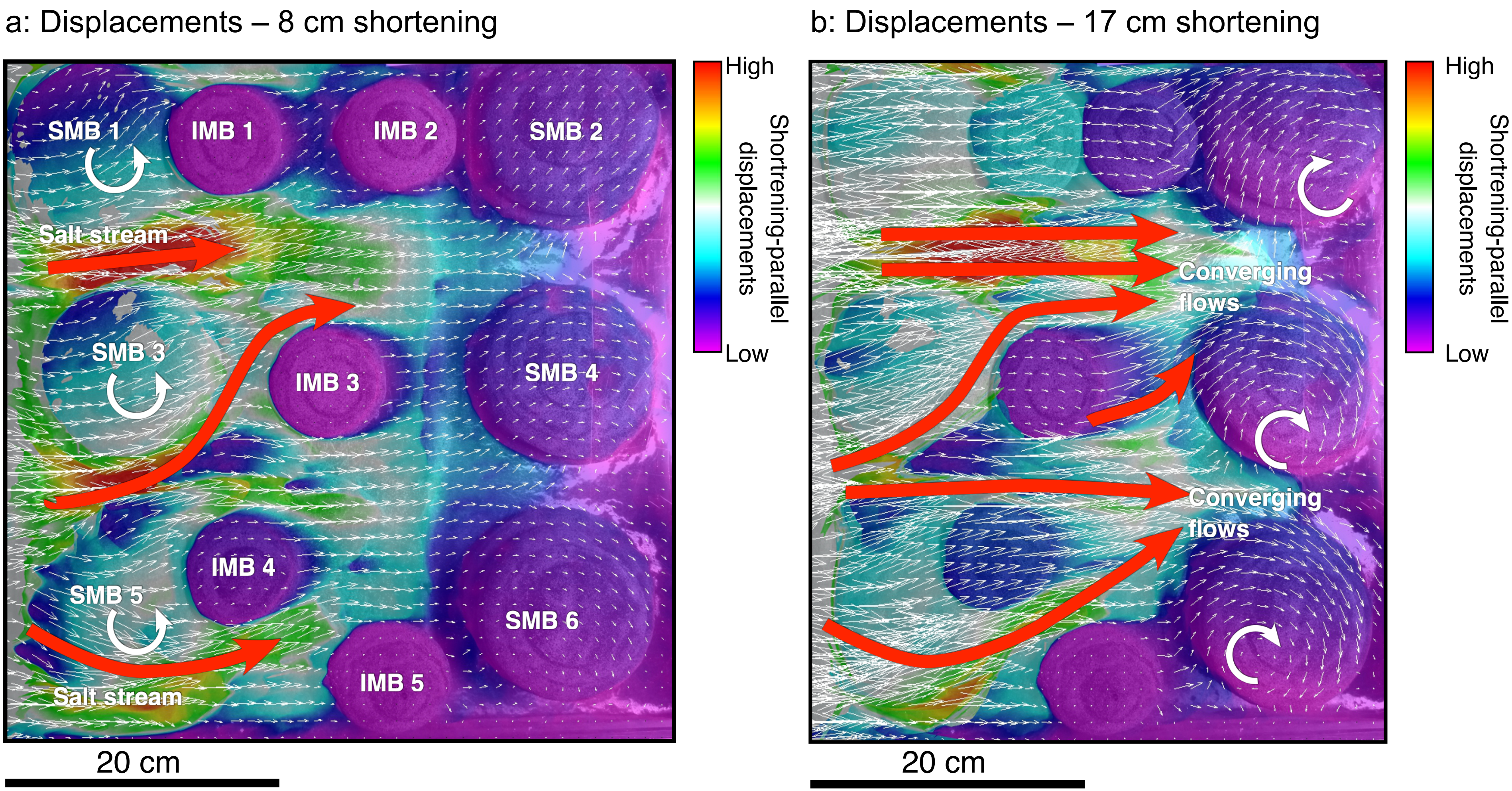
a: Displacements – 8 cm shortening
SMB 1
IMB 1
IMB 2
SMB 2
Salt stream
SMB 3
IMB 3
SMB 4
IMB 4
SMB 5
SMB 6
IMB 5
Salt stream
20 cm
High
Low
Shortrening-parallel displacements
b: Displacements – 17 cm shortening
Converging flows
Converging flows
20 cm
High
Low
Shortrening-parallel displacements

Figure 15

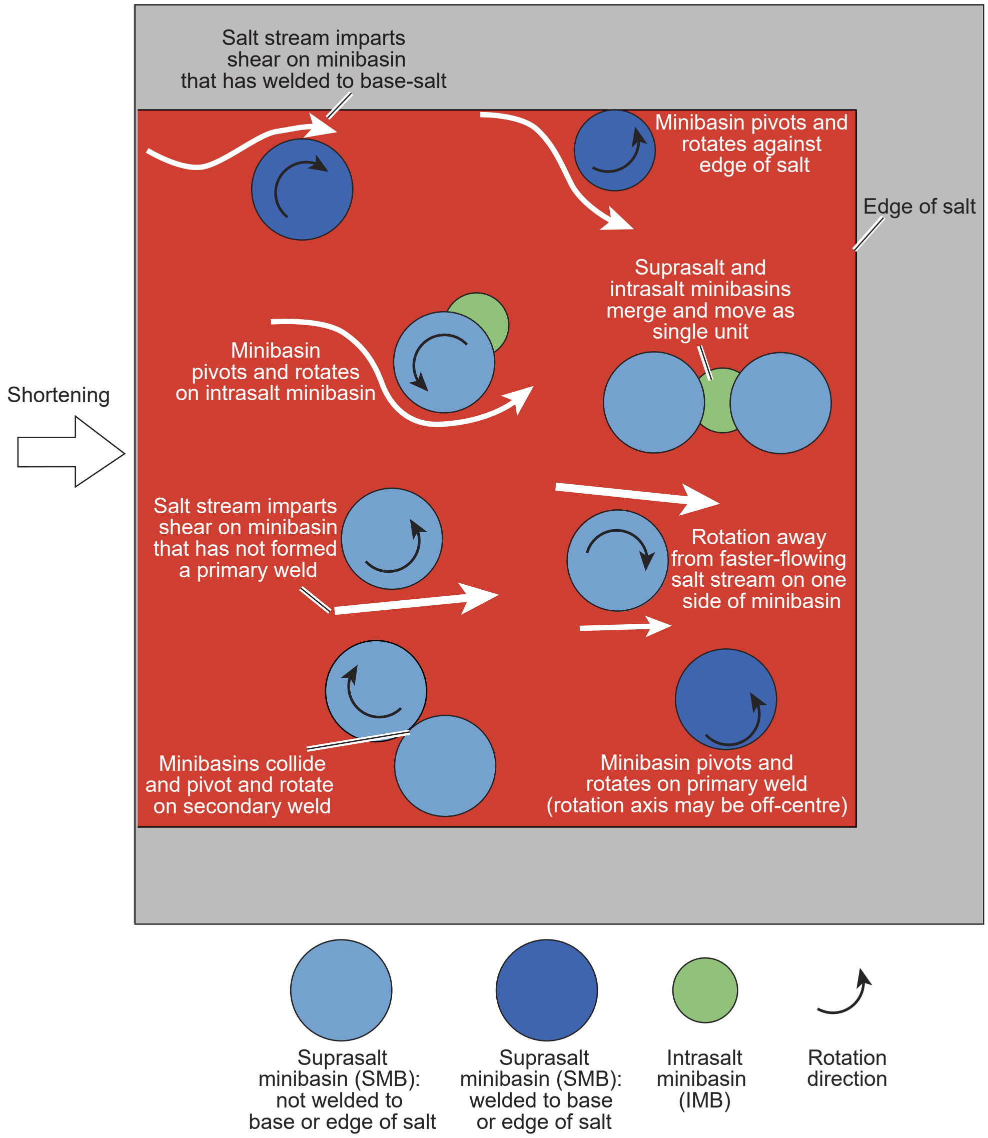
Salt stream imparts shear on minibasin that has welded to base-salt
Minibasin pivots and rotates against edge of salt
Edge of salt
Suprasalt and intrasalt minibasins merge and move as single unit
Minibasin pivots and rotates on intrasalt minibasin
Shortening
Salt stream imparts shear on minibasin that has not formed a primary weld
Rotation away from faster-flowing salt stream on one side of minibasin
Minibasins collide and pivot and rotate on secondary weld
Minibasin pivots and rotates on primary weld (rotation axis may be off-centre)
Suprasalt minibasin (SMB): not welded to base or edge of salt
Suprasalt minibasin (SMB): welded to base or edge of salt
Intrasalt minibasin (IMB)
Rotation direction

Figure 16a

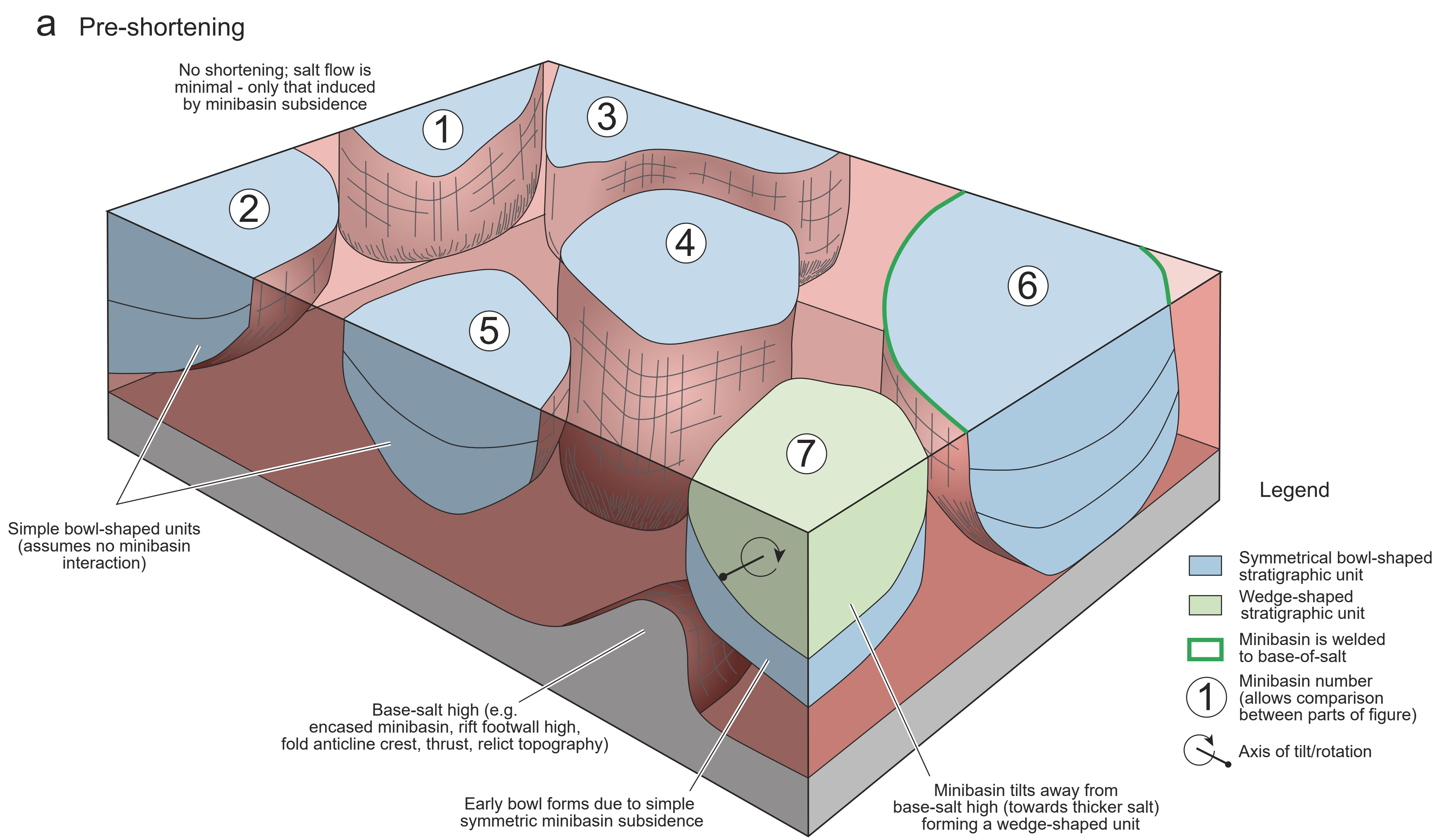
a Pre-shortening
No shortening; salt flow is minimal - only that induced by minibasin subsidence
1
2
3
4
5
6
7
Simple bowl-shaped units (assumes no minibasin interaction)
Base-salt high (e.g. encased minibasin, rift footwall high, fold anticline crest, thrust, relict topography)
Early bowl forms due to simple symmetric minibasin subsidence
Minibasin tilts away from base-salt high (towards thicker salt) forming a wedge-shaped unit
Legend
Symmetrical bowl-shaped stratigraphic unit
Wedge-shaped stratigraphic unit
Minibasin is welded to base-of-salt
Minibasin number (allows comparison between parts of figure)
Axis of tilt/rotation

Figure 16b

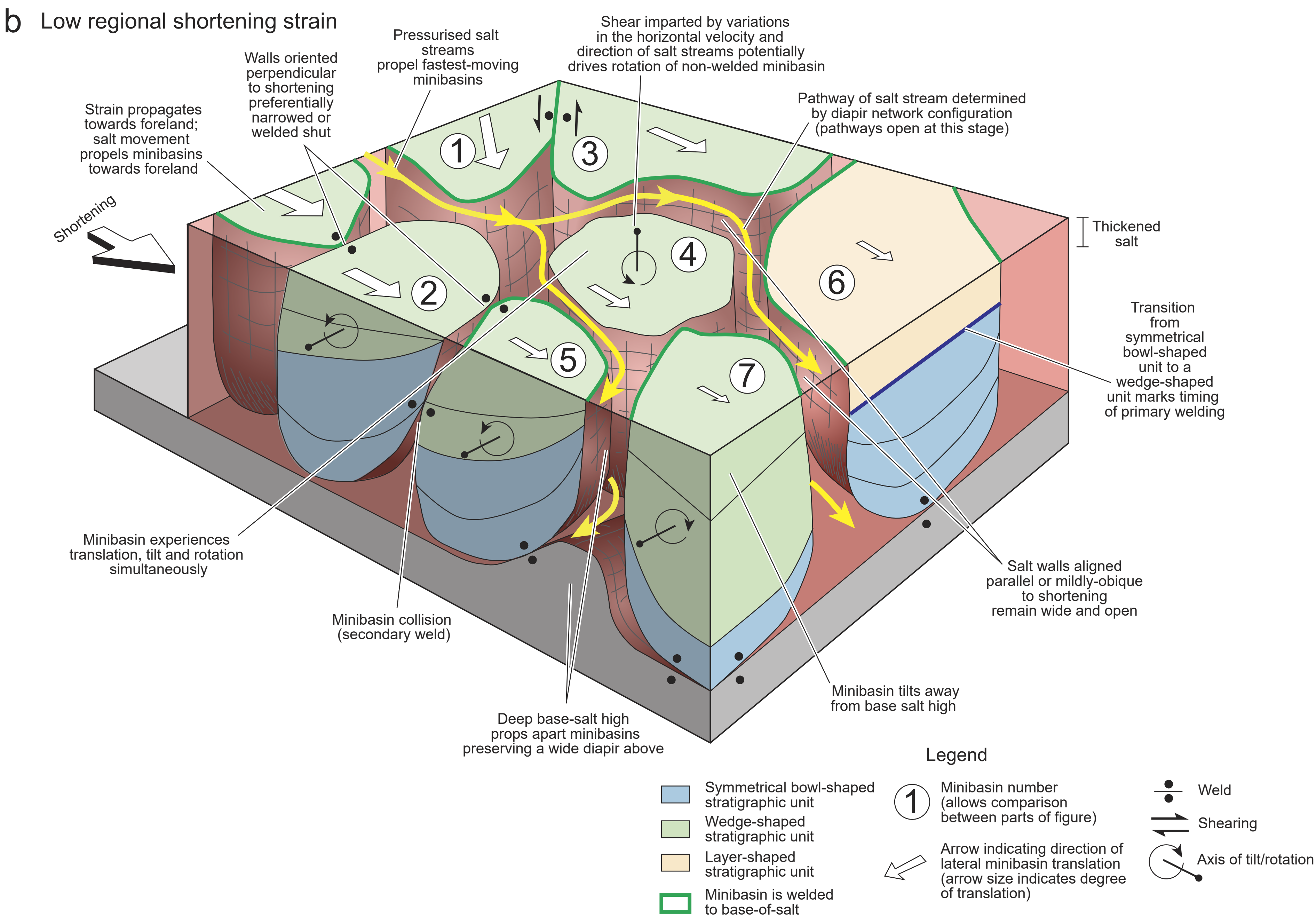
b Low regional shortening strain
Strain propagates towards foreland; salt movement propels minibasins towards foreland
Walls oriented perpendicular to shortening preferentially narrowed or welded shut
Pressurised salt streams propel fastest-moving minibasins
Shear imparted by variations in the horizontal velocity and direction of salt streams potentially drives rotation of non-welded minibasin
Pathway of salt stream determined by diapir network configuration (pathways open at this stage)
Shortening
1
2
3
4
5
6
7
Thickened salt
Transition from symmetrical bowl-shaped unit to a wedge-shaped unit marks timing of primary welding
Minibasin experiences translation, tilt and rotation simultaneously
Minibasin collision (secondary weld)
Deep base-salt high props apart minibasins preserving a wide diapir above
Minibasin tilts away from base salt high
Salt walls aligned parallel or mildly-obique to shortening remain wide and open
Legend
Symmetrical bowl-shaped stratigraphic unit
Wedge-shaped stratigraphic unit
Layer-shaped stratigraphic unit
Minibasin is welded to base-of-salt
Minibasin number (allows comparison between parts of figure)
Arrow indicating direction of lateral minibasin translation (arrow size indicates degree of translation)
Weld
Shearing
Axis of tilt/rotation

Figure 16c

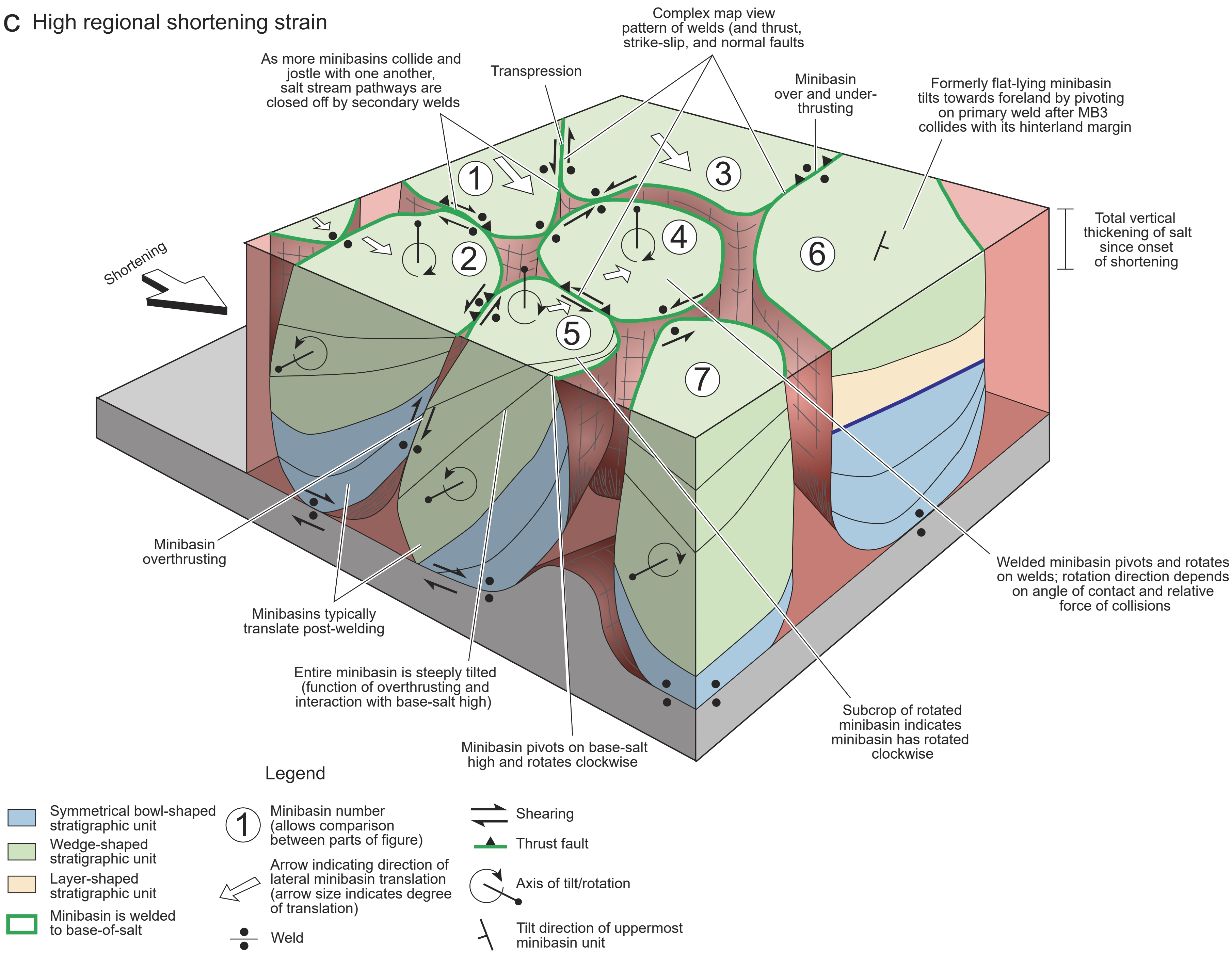
C High regional shortening strain
Complex map view pattern of welds (and thrust, strike-slip, and normal faults
As more minibasins collide and jostle with one another, salt stream pathways are closed off by secondary welds
Transpression
Minibasin over and under-thrusting
Formerly flat-lying minibasin tilts towards foreland by pivoting on primary weld after MB3 collides with its hinterland margin
Total vertical thickening of salt since onset of shortening
Shortening
1
2
3
4
5
6
7
Minibasin overthrusting
Minibasins typically translate post-welding
Entire minibasin is steeply tilted (function of overthrusting and interaction with base-salt high)
Minibasin pivots on base-salt high and rotates clockwise
Subcrop of rotated minibasin indicates minibasin has rotated clockwise
Welded minibasin pivots and rotates on welds; rotation direction depends on angle of contact and relative force of collisions
Legend
Symmetrical bowl-shaped stratigraphic unit
Wedge-shaped stratigraphic unit
Layer-shaped stratigraphic unit
Minibasin is welded to base-of-salt
Minibasin number (allows comparison between parts of figure)
Arrow indicating direction of lateral minibasin translation (arrow size indicates degree of translation)
Weld
Shearing
Thrust fault
Axis of tilt/rotation
Tilt direction of uppermost minibasin unit

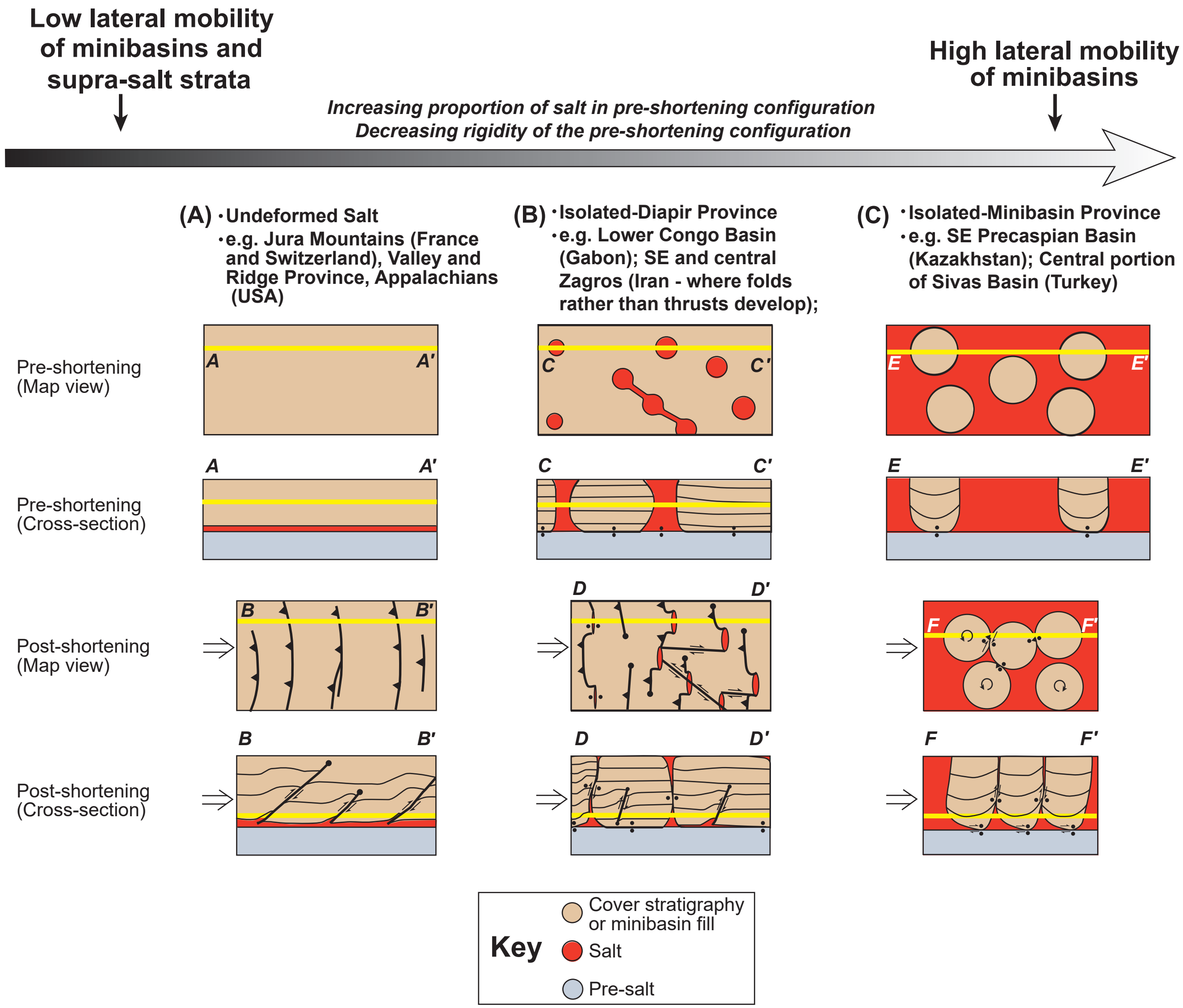
Low lateral mobility of minibasins and supra-salt strata
High lateral mobility of minibasins
Increasing proportion of salt in pre-shortening configuration
Decreasing rigidity of the pre-shortening configuration
(A) •Undeformed Salt
•e.g. Jura Mountains (France and Switzerland), Valley and Ridge Province, Appalachians (USA)
(B) •Isolated-Diapir Province
•e.g. Lower Congo Basin (Gabon); SE and central Zagros (Iran - where folds rather than thrusts develop);
(C) •Isolated-Minibasin Province
•e.g. SE Precaspian Basin (Kazakhstan); Central portion of Sivas Basin (Turkey)
Pre-shortening (Map view)
Pre-shortening (Cross-section)
Post-shortening (Map view)
Post-shortening (Cross-section)
A
A'
C
C'
E
E'
B
B'
D
D'
F
F'
Key
Cover stratigraphy or minibasin fill
Salt
Pre-salt